bioRxiv preprint doi: https://doi.org/10.1101/2020.09.28.283952; this version posted September 29, 2020. The copyright holder for this preprint (which was not certified by peer review) is the author/funder. All rights reserved. No reuse allowed without permission.

Cerebellar Activation Bidirectionally Regulates Nucleus Accumbens Shell and Core

Alexa D'Ambra[1], Se Jung Jung[1], Swetha Ganesan[1#], Evan G. Antzoulatos[1,2a], Diasynou Fioravante[1,2a*]

[1]Center for Neuroscience, [2]Department of Neurobiology, Physiology and Behavior, University of California Davis, United States

[a]These authors share senior authorship

[#]Current address:
Gillins School of Global Public Health
University of North Carolina

*Correspondence should be addressed to:
Diasynou Fioravante, PhD
E-mail: dfioravante@ucdavis.edu

bioRxiv preprint doi: https://doi.org/10.1101/2020.09.28.283952; this version posted September 29, 2020. The copyright holder for this preprint (which was not certified by peer review) is the author/funder. All rights reserved. No reuse allowed without permission.

Abstract

Traditionally viewed as a motor control center, the cerebellum (CB) is now recognized as an integral part of a broad, long-range brain network that serves limbic functions and motivates behavior. This diverse CB functionality has been at least partly attributed to the multiplicity of its outputs. However, relatively little attention has been paid to CB connectivity with subcortical limbic structures, and nothing is known about how the CB connects to the nucleus accumbens (NAc), a complex striatal region with which the CB shares functionality in motivated behaviors. Here, we report findings from in vivo electrophysiological experiments that investigated the functional connectivity between CB and NAc. We found that electrical microstimulation of deep cerebellar nuclei (DCN) modulates NAc spiking activity. This modulation differed in terms of directionality (excitatory vs. inhibitory) and temporal characteristics, in a manner that depends on NAc subregions: in the medial shell of NAc (NAc_{Med}), slow inhibitory responses prevailed over excitatory ones, whereas the proportion of fast excitatory responses was greater in the NAc core (NAc_{Core}) compared to NAc_{Med}. Slow inhibitory modulation of NAc_{Core} was also observed but it required stronger CB inputs compared to NAc_{Med}. Finally, we observed shorter onset latencies for excitatory responses in NAc_{Core} than in NAc_{Med}, which argues for differential connectivity. If different pathways provide signal to each subregion, the divergence likely occurs downstream of the CB because we did not find any response-type clustering within DCN. Because there are no direct monosynaptic connections between CB and NAc, we performed viral tracing experiments to chart disynaptic pathways that could potentially mediate the newly discovered CB-NAc communication. We identified two anatomical pathways that recruit the ventral tegmental area and intralaminar thalamus as nodes. These pathways and the functional connectivity they support could underlie CB's role in motivated behaviors.

Keywords

Cerebellum, nucleus accumbens, ventral striatum, connectivity, mouse, electrophysiology, anatomy, circuit, thalamus, intralaminar, VTA, motivated behavior, non-motor

bioRxiv preprint doi: https://doi.org/10.1101/2020.09.28.283952; this version posted September 29, 2020. The copyright holder for this preprint (which was not certified by peer review) is the author/funder. All rights reserved. No reuse allowed without permission.

Introduction

The cerebellum (CB) exploits the parallel, modular organization of its circuitry to integrate information and perform complex computations. Most CB research sheds light on this complexity in the context of CB's role in predicting and updating motor movements[1]. However, accumulating evidence supports CB involvement in high-order non-motor functions as well[2–5]. In humans, the CB is consistently activated during decision making, particularly during risk- or reward-based tasks[6,7], and during aversive experiences and emotional learning[8,9]. Further support for non-motor CB roles stems from clinical translational studies, which have linked CB dysfunction with neurodevelopmental disorders, posttraumatic stress disorder, generalized anxiety disorder, addiction, and cognitive and emotional disturbances known as cerebellar cognitive affective syndrome[8,10–18]. These findings are further corroborated by evidence from animal studies, which solidify a role for the CB in the processing of valence, reward, reward anticipation and omission[19–23]; emotional learning and aggression[24–30]; and motivation[31–33].

The ability of the CB to derive a complex repertoire of non-motor functions from its relatively invariant cellular organization is largely attributed to its diverse outputs[34,35]. In addition to the heavily emphasized non-motor cerebellar influences on cortical regions[36–42], functional and/or anatomical CB connections with subcortical structures critical for cognition and emotion have also been documented[43–48]. Here, we focused on the nucleus accumbens (NAc), a complex limbic structure that shares reward, motivation and affective functionality with the CB[49,50]. Stimulation of CB cortex or deep cerebellar nuclei (DCN) modulates levels of NAc dopamine- an important, but not exclusive, regulator of NAc functions[51–57]. However, how the CB connects to NAc is unknown.

Here we used in vivo electrophysiology in anesthetized mice to examine the effects of CB stimulation on spiking activity in the NAc medial shell (NAc_{Med}) and core (NAc_{Core}). These regions exhibit distinct input-output organization, anatomy, and function[58–63]. We provide the first evidence, to our knowledge, of an electrophysiological connection between CB and NAc, which shows NAc subregion-dependent specificity. Using viral tracing approaches, we offer first insights on the anatomical blueprint of CB-NAc connectivity, which includes nodal neurons in ventral tegmental area (VTA) and limbic thalamus. These findings may expound upon the CB's involvement in limbic functions such as motivation, reward learning, and affective processing.

bioRxiv preprint doi: https://doi.org/10.1101/2020.09.28.283952; this version posted September 29, 2020. The copyright holder for this preprint (which was not certified by peer review) is the author/funder. All rights reserved. No reuse allowed without permission.

Materials and Methods

In vivo electrophysiology

Mice

C57Bl/6J mice of both sexes (N = 29) were used in accordance with the National Institutes of Health guidelines and the policies of the University of California Davis Committee for Animal Care. Acute in vivo recordings were performed at postnatal days P21-P29. All animals were maintained on a light/dark cycle (light 7AM-7PM), and experiments were performed during the light cycle.

Surgery

Anesthesia was initially induced by brief inhalation of 4-5% isoflurane followed by an intraperitoneal injection of anesthetic cocktail (100 mg/kg Ketamine; 10 mg/kg xylazine; 1 mg/kg acepromazine), and was maintained with periodic injections of the anesthetic cocktail (20-50 mg/kg ketamine), as needed. Animals were placed in a stereotactic frame after confirmation of anesthesia depth using a toe pinch response test. Breathing rate and toe pinch responses were monitored to ensure maintenance of anesthesia. A small craniotomy and durectomy were performed over the DCN (lateral/interposed n.: relative to lambda, in mm: -2.1 to - 2.6 AP; +/-2.1 to +/-2.3 ML), and over NAc targeting the medial shell and/or core (relative to bregma: +1.7 to +1.54 AP; +/- 0.4 to +/-1.15 ML).

Stimulation

A custom stimulating stereotrode (~200 μm distance between tips) was lowered 1.95 – 2.45 mm below the brain surface (in DV axis) through the cerebellar craniotomy to reach the DCN. Ten trials of bipolar constant-current electrical microstimulation were delivered at each location at a 15-s inter-trial interval. Each stimulation trial consisted of a 200-Hz burst of five 0.5-ms monophasic square-waveform pulses at 100 μA. In a subset of experiments (N = 11 mice), the stimulation intensity was varied between 30, 100, and 300 μA in interleaved blocks of 5 trials per intensity. The use of stereotrode-delivered electrical stimuli in these experiments was instrumental in allowing us to 1) probe changes in NAc spiking activity in response to broad variations in current intensity; 2) exercise tight control over a small localized area; 3) simultaneously stimulate all neurons in that area.

Data Acquisition

bioRxiv preprint doi: https://doi.org/10.1101/2020.09.28.283952; this version posted September 29, 2020. The copyright holder for this preprint (which was not certified by peer review) is the author/funder. All rights reserved. No reuse allowed without permission.

For electrophysiological recordings, a 12-channel (platinum; 0.2-2 MΩ impedance) axial multi-electrode array (FHC; 150 µm distance between channels), dipped in fluorescein dextran (3000 MW), was lowered into the NAc at a depth of 3.75 – 5.25 mm below the brain surface (DV axis). Electrode signals were fed to a digital headstage (RHD 2132, Intan Technologies) for amplification (x20), filtering (0.7-7500 Hz) and digitization (30 kS/s with 16-bit resolution), before transfer to an open-source acquisition system (OpenEphys) for display and storage.

Histology for Verification of Electrode Placement

Positioning of electrodes was initially guided by atlas-based stereotactic coordinates (Paxinos & Franklin) and, upon completion of experiments, histologically verified through electrolytic lesions (for location of DCN microstimulation electrodes; single 10-s cathodal pulse of 300 µA) and fluorescence imaging (NAc fluorescein dye track). Coordinates for subsequent animals of the same litter were further adjusted accordingly. Briefly, at the end of experiments electrodes were retracted and animals were perfused with 4% (w/v) paraformaldehyde (PFA) in 0.1 M phosphate buffer (PB). Brains were dissected and post-fixed in 4% PFA, sliced in phosphate buffered saline (PBS) and inspected under a fluorescence stereoscope (Olympus SZX2). NAc slices containing the dye track from the recording array were identified under 488 nm light, and CB slices with electrolytically lesioned tissue were identified under brightfield illumination. Slices of interest were subsequently stained with DAPI (1 : 20,000, Thermo Fisher Scientific), mounted on slides, and imaged using a VS120 Olympus slide scanner. Images were manually registered to the Paxinos and Franklin Mouse Brain Atlas and the location of the recording electrode tip was mapped. Only channels along the recording array that were determined to be within NAc_{Med} and/or NAc_{Core} were included in analysis. Similarly, experiments in which cerebellar electrolytic lesions were localized outside the lateral and/or interposed DCN were excluded from analysis.

Quantification and Statistical Analysis

Data processing and quantification

Custom-written MATLAB scripts (Mathworks) were used for data processing and analysis. Separation of multi-unit spikes from local field potentials was achieved through a 4th-order Butterworth high-pass filter (cutoff at 300 Hz). The filtered signal was thresholded at 3-3.5 standard deviations below the average voltage of a 10-s baseline (taken before stimulation

bioRxiv preprint doi: https://doi.org/10.1101/2020.09.28.283952; this version posted September 29, 2020. The copyright holder for this preprint (which was not certified by peer review) is the author/funder. All rights reserved. No reuse allowed without permission.

onset), and neural firing rates were computed from the spike counts in consecutive 10-ms time bins (peri-stimulus time histogram; PSTH). Putative spikes with time differences less than 10 ms from stimulus artifacts or 2 ms from the previous spike were discarded.

To quantify the DCN stimulation-induced modulation of NAc spiking activity we first averaged the PSTH across all trials of the same intensity at the same recording and stimulation sites, and randomly permuted a trial-averaged 10-s pre-stimulus baseline 1,000 times. The observed trial-averaged PSTH was then z-transformed based on the mean and standard deviation of the randomization distribution (z-transformed firing rate). A change of firing rate from baseline was considered a response to DCN stimulation only if it (a) took place within the first 3 s following stimulus onset (response window), and (b) exceeded either a positive threshold of z = 4 (for excitatory responses) or a negative threshold of z = -3.2 (for inhibitory responses). The same thresholds were employed to identify responses of both NAc subregions and to all stimulation intensities that were tested in this study. Recordings with responses were categorized as responders (vs. non-responders). Extensive analyses of candidate thresholds (an example subset of the candidate thresholds we tested appears in Fig. 2S1) allowed us to employ response thresholds that (a) kept the relative frequency of threshold crossings during a 3-s pre-stimulus baseline window (i.e., same duration as the response window) less than 5% (false positive responses; typically around 2-3%), and (b) the relative distribution of excitatory/inhibitory responses was robust to small changes in threshold. Onset latency of responses was quantified as the time of threshold crossing relative to stimulus onset.

Statistics

Unless otherwise noted, we performed all statistical comparisons using the random permutation method[64,65]. We randomly shuffled the data between groups 1,000 times and estimated the probability to find a difference greater than or equal to the observed difference by chance alone. We corrected for multiple comparisons with False Discovery Rate (FDR)[66] set at 10%.

Anatomical Tracing

Surgery and viral injections

bioRxiv preprint doi: https://doi.org/10.1101/2020.09.28.283952; this version posted September 29, 2020. The copyright holder for this preprint (which was not certified by peer review) is the author/funder. All rights reserved. No reuse allowed without permission.

Mice of both sex (P35 - P49) were anesthetized with isoflurane (4 % - 5 % induction; 1.5 % maintenance) and secured to a stereotactic frame. After exposing the top of the skull, the head was leveled and small craniotomies were drilled over areas of interest. Injections were made using a Micro4 controller and UltraMicroPump 3 (VWR). Glass needles were made from 1-mm outer diameter glass pipettes (Wiretrol II, Drummond) pulled to a fine tip (20 - 50 µm tip diameter, 3 - 4 mm tip length) using a pipette puller (P-97, Sutter). Needles were left in place for 7-10 min following injections to minimize diffusion. Following surgery and analgesia administration (0.1 mg/kg buprenorphine, 5 mg/kg meloxicam), mice were allowed to recover on a warm heating pad before being transferred back to the vivarium. Mice remained in the colony to allow for recovery and retrograde labeling/virus expression for 2-3 weeks prior to euthanasia and tissue collection/processing.

For co-localization experiments (Fig. 6): AAV9-CAG-GFP (2 x 10^{12} viral particles/ml, UNC viral core) was injected in DCN (from bregma, in mm: medial n.: -2.55 AP, ± 0.75 ML, -2.1 DV, 50 nl; interposed n. : -2.5 AP, ± 1.55 ML, -2.1 DV, 50 nl; lateral n.: -2.2 AP, ± 2.3 ML, -2.12 DV, 50 nl; and -1.8, ± 2.35 ML, -2.12 DV, 50 nl). Cholera toxin subunit B (ctb)- 640 or -568 (5 mg/ml, Biotium) was injected in NAc shell and core (from bregma, in mm: 1.8 AP, ± 0.8 ML, -4.2 DV, 200 nl). For anterograde transsynaptic tracing (Fig. 7): AAV1-hSyn-Cre-WPRE-hGH (10^{13} gc/ml, Addgene; 1:10 dilution) was injected in DCN (coordinates as above). AAV5-CAG-FLEX-tdTomato (7.8 x 10^{12} viral particles/ml, UNC viral core; 1 : 2 dilution) or AAV5-pCAG-FLEX-EGFP-WPRE (1.1 x 10^{13} gc/ml, Addgene; 1 : 2 dilution) was injected in VTA (from bregma, in mm: 2.8 AP, ± 0.35 ML, -4.2 DV, 100 nl; and -2.85 AP, ± 0.6 ML, -4.2 DV, 100 nl) or thalamus (from bregma, in mm: -0.85 AP, ± 0.3 ML, -3.3 DV, 300 nl; and -1.2 AP, ± 0.5 ML, -3.5 DV, 300 nl; 1:5 dilution).

Histology and fluorescence microscopy

Two to three weeks following tracer/virus injections, mice were anesthetized with an anesthetic cocktail (100 mg/kg ketamine, 10 mg/kg xylazine, 1 mg/kg acepromazine) and perfused transcardially with 4 % (w/v) PFA in PB. Brains were post-fixed in 4 % PFA for 6 h and transferred to 30 % sucrose in PBS for overnight incubation at 4 °C. Brains were coronally sectioned (60 µm) on a sliding microtome, stained with DAPI, mounted to slides, coverslipped with Mowiol-based antifade solution and imaged. VTA sections were immunostained for

bioRxiv preprint doi: https://doi.org/10.1101/2020.09.28.283952; this version posted September 29, 2020. The copyright holder for this preprint (which was not certified by peer review) is the author/funder. All rights reserved. No reuse allowed without permission.

tyrosine hydroxylase (TH) prior to mounting, as follows: slices were first incubated with blocking solution [10 % normal goat serum (NGS) in PBS supplemented with 0.3 % Triton-X100; PBST] for 1 h at room temperature, then with mouse anti-TH (clone LNC11, Millipore Sigma; 1 : 1000) in blocking solution with 2 % NGS overnight at 4 ^{o}C. Sections were washed with PBST (3 x 20 min) and incubated for 1 h at room temperature with goat anti-mouse Alexa fluor 488 secondary antibody (1 : 1000), washed with PBS (3 x 20 min), mounted, coverslipped and imaged. Epifluorescence image mosaics were acquired on an Olympus VS120 slide scanner with a 10x air objective. High magnification confocal images were taken sequentially with different laser lines and a 60x oil-immersion objective on a Zeiss LSM800 microscope with Airyscan. Image brightness/contrast was adjusted using ImageJ (NIH) for display purposes.

Results

DCN microstimulation bidirectionally alters NAc spiking activity

To examine functional connectivity between CB and NAc, we recorded ongoing spiking activity from NAc_{Med} and NAc_{Core} *in vivo* and electrically microstimulated the DCN (Figure 1A,B). We primarily targeted the lateral DCN, activation of which has been shown to modulate levels of dopamine in NAc[53]. In a subset of experiments, post-hoc analysis localized the bipolar stimulating electrode in the interposed DCN, and these data were included in our analysis. Activation of DCN with 100-μA current pulses evoked two distinct types of responses in NAc: inhibitory (Fig. 1C) and excitatory (Fig. 1D). We define a response as the positive and/or negative threshold-crossing spiking activity that occurred within 3 s from stimulus presentation. The time course of all positive (*blue*) and negative (*red*) threshold-crossing spiking activity throughout the 10 s trial can be seen in the peri-stimulus time histograms in Fig. 2 (Fig. 2A1 and 2A2). Analysis of NAc responses revealed differences in the prevalence of each response type (i.e., inhibitory vs. excitatory), based on NAc subregion. In NAc_{Med}, DCN microstimulation elicited a significant number of inhibitory responses compared to pre-stimulus baseline (Fig. 2B,C)(proportion of inhibitory responses in NAc_{Med}: 16.7 %, comparison to pre-stimulus baseline activity: $p = 0.0$), as well as some excitatory responses (6.1 %)(Fig. 2B); however, the proportion of the latter did not differ significantly from that expected by chance alone ($p = 0.18$)(Fig. 2C). By contrast, DCN microstimulation elicited a significant number of both inhibitory and excitatory responses in NAc_{Core} (Fig. 2B,C; 17.1 % inh.: $p = 0.0$; 13.7 % excit.: $p = 0.003$). There was no significant difference between the prevalence of all (pooled excitatory

bioRxiv preprint doi: https://doi.org/10.1101/2020.09.28.283952; this version posted September 29, 2020. The copyright holder for this preprint (which was not certified by peer review) is the author/funder. All rights reserved. No reuse allowed without permission.

and inhibitory) responses between the two subregions (p = 0.11), or between the proportion of excitatory and inhibitory responses in NAc_{Core} (p = 0.14). Finally, there was no difference in the proportion of inhibitory responses between NAc_{Med} and NAc_{Core} (p = 0.55) (Table 1A-E).

To ensure that the observed relationships between excitatory and inhibitory responses in NAc_{Med} and NAc_{Core} did not hinge on response thresholds, we quantified proportions of responses for different threshold values (Fig. 2S1). We chose values that maintained a maximum of 5 % threshold crossings during pre-stimulus baseline (i.e., false positive response rate of 5 %). We found that the relative distribution of excitatory and inhibitory responses was robust to small changes in threshold. Together, these results suggest that (a) activation of DCN can modulate ongoing spiking activity in NAc and (b) this modulation is both inhibitory and excitatory. Interestingly, (c) excitatory modulation of spiking activity is more prevalent in NAc_{Core} than in NAc_{Med}; and (d) in NAc_{Med}, inhibitory modulation is more prevalent than excitatory.

Temporal profiles of NAc responses

We evaluated the temporal profiles of NAc responses. In both NAc_{Med} and NAc_{Core}, excitatory responses appeared to precede inhibitory ones (Fig. 2A1,A2). This can be seen more clearly in 3D color plots (Fig. 3A,B), in which all excitatory and inhibitory responders are aligned to the time of stimulus onset and ordered by response-onset latency, with the z-transformed firing rate represented by color (corresponding color plots of all non-responders ordered by latency of peak activity are shown in Fig. 3S1). To quantitatively describe these differences, we compared onset latencies for excitatory and inhibitory responses using multiple-comparison-corrected random permutation tests (Fig. 3C and Table 1F,G). We found that excitatory responses were significantly faster (i.e., had shorter onset latencies) than inhibitory ones both in NAc_{Med} (mean ± SEM: excit.: 0.63 ± 0.33 s, inh.: 1.24 ± 0.15 s, p = 0.03) and in NAc_{Core} (mean ± SEM: excit.: 0.12 ± 0.02 s, inh.: 1.08 ± 0.14 s, p = 0.0). Moreover, excitatory responses were faster in NAc_{Core} than in NAc_{Med} (p = 0.048), whereas the onset latency of inhibitory responses did not differ significantly between the two subregions (p = 0.22).

To evaluate the time period over which NAc spiking activity remained supra-threshold, we plotted the cumulative probability of threshold crossings in NAc_{Med} and NAc_{Core} excitatory and

bioRxiv preprint doi: https://doi.org/10.1101/2020.09.28.283952; this version posted September 29, 2020. The copyright holder for this preprint (which was not certified by peer review) is the author/funder. All rights reserved. No reuse allowed without permission.

inhibitory responders as a function of time from stimulus onset (Fig. 3D1,D2). These plots are also informative of how fast, and presumably synchronous, the initial rise in activity was. This approach does not impose a theoretical model on the data, which may or may not be fitted adequately by the model, in order to extract information on temporal characteristics. We found that excitatory responses were indeed faster and shorter-lived than inhibitory responses in both NAc subregions [50 % rise-time (in s): NAc_{Med}: excit.: 0.22; inh.: 1.795, permutation test, p = 0.01; NAc_{Core}: excit.: 0.175, inh.: 1.195, permutation test, p = 0.0]. The 50 % rise-times of excitatory responses in NAc_{Med} and NAc_{Core} were not significantly different (p = 0.36), despite the few threshold crossings observed at later time points (Fig. 3D1). Finally, the small difference between NAc_{Med} and NAc_{Core} inhibitory responses (Fig. 3D2) did not reach significance (p = 0.06) (Table 1H). Collectively, these results suggest that DCN microstimulation reliably evokes fast, short-lived excitatory responses in NAc_{Core}, as well as slower and temporally protracted inhibitory responses in NAc_{Med} and NAc_{Core}.

Spatial considerations for electrical stimulation

To maintain fine control of electrical current spread at DCN stimulation sites, we used bipolar stimulation electrodes. To confirm that the stimulation was indeed localized, we performed current-spread analysis (Fig. 4D), which took advantage of the fact that we probed individual NAc recording sites with stimuli delivered at multiple DCN sites. We quantified the likelihood that stimulation of a DCN site would evoke a significant excitatory or inhibitory response in a NAc site and plotted it as a function of the Euclidean distance from the DCN site that evoked the strongest response in that NAc site (most effective DCN stimulation site, at d = 0 µm). We reasoned that if the electrical current spread over a large radius from the most effective DCN site, stimulation of other sites within that radius would also evoke NAc responses with likelihood greater than expected by chance. We found that even at close distances (100 µm) from the most effective site, the probability of a DCN stimulation site evoking a significant response was not different from the marginal probability (i.e., the probability to evoke a response across all recordings, regardless of distance from the most effective site) (p = 0.45) (Table 1I). This result confirms that our stimulation was localized.

Given that DCN stimulation was localized, could the observed differences in NAc response types arise from regional differences within DCN? To address this question, we

bioRxiv preprint doi: https://doi.org/10.1101/2020.09.28.283952; this version posted September 29, 2020. The copyright holder for this preprint (which was not certified by peer review) is the author/funder. All rights reserved. No reuse allowed without permission.

examined whether there was clustering of DCN sites with respect to their effectiveness to evoke significant excitatory or inhibitory responses in NAc_{Med} and/or NAc_{Core}. We did not find indications of such clustering (Fig. 4B,C), which argues against topographical organization of lateral DCN with respect to NAc response types. Using a similar approach, we examined whether there was topographical clustering of excitatory and/or inhibitory responder sites within NAc subregions, but we did not find evidence for any such organization either (not shown).

Differential and non-linear dependence of NAc responses on DCN stimulation intensity

To further probe the functional connectivity between DCN and NAc, in a subset of experiments we assessed the effectiveness of DCN microstimulation to modulate spiking activity in NAc_{Med} and NAc_{Core} at three different intensities: 30 μA, 100 μA, and 300 μA. We found that the roughly 3-fold changes in stimulation intensity had (a) differential effects based on response type and NAc subregion, and (b) non-linear effects on the prevalence of response types in both NAc subregions.

Specifically, weak (30 μA) DCN stimulation effectively evoked a small but significantly greater-than-baseline number of only inhibitory responses and only in NAc_{Med} (Fig. 5A,B) (proportion of responses: NAc_{Med}: inh.: 7.5 %; compared to pre-stimulus baseline, $p = 0.03$; exc.: 10.5 %, compared to pre-stimulus baseline, $p = 0.07$; excit. vs. inh: $p = 0.61$; NAc_{Core}: inh.: 1.5 %, compared to pre-stimulus baseline, $p = 0.5$; exc.: 8.7 %, compared to pre-stimulus baseline, $p = 0.14$) (Table 2A-B,D). Even after increasing intensity to 100 μA, only inhibitory responses could be evoked reliably above baseline in NAc_{Med} (proportion of responses: inh.: 15.8 %, compared to pre-stimulus baseline, $p = 0.0$; exc.: 3.2 %, compared to pre-stimulus baseline, $p = 0.64$; exc. vs. inh.: $p = 0.02$). In contrast, in NAc_{Core} 100-μA DCN stimulation evoked significant proportions of both inhibitory and excitatory responses (inh.: 19.8 %, compared to pre-stimulus baseline, $p = 0.0$; exc.: 11.9 %, compared to pre-stimulus baseline, $p = 0.01$) (exc. vs. inh.: $p = 0.01$). The differential effect of 100-μA microstimulation on NAc subregions was statistically significant: more excitatory responses were evoked in NAc_{Core} than in NAc_{Med} ($p = 0.02$), whereas the prevalence of inhibitory responses was similar between subregions ($p = 0.29$). Finally, the 300-μA DCN microstimulation evoked significant proportions of both inhibitory and excitatory responses in NAc_{Med} (inh.: 13.1 %, compared to pre-stimulus

bioRxiv preprint doi: https://doi.org/10.1101/2020.09.28.283952; this version posted September 29, 2020. The copyright holder for this preprint (which was not certified by peer review) is the author/funder. All rights reserved. No reuse allowed without permission.

baseline, p = 0.0; exc.: 19.1 %, compared to pre-stimulus baseline, p = 0.003; exc. vs. inh.: p = 0.4), as well as in NAc_{Core} (inh.: 17.3 %, compared to pre-stimulus baseline, p = 0.004; exc.: 24 %, compared to pre-stimulus baseline, p = 0.0)(exc. vs. inh.: p = 0.0), with no significant difference between the two subregions (p = 0.28 for excit. in NAc_{Med} vs. NAc_{Core}; p = 0.29 for inh. in NAc_{Med} vs. NAc_{Core}) (Table 2A-E).

The non-linear effects of stimulation intensity can be appreciated if we consider the change in the prevalence of response types across different intensities (Fig. 5B; Table 2F). In both NAc_{Med} and NAc_{Core}, increasing stimulation intensity from 30 μA to 100 μA did not significantly increase excitatory responses. In fact, in NAc_{Med} we observed a strong trend toward fewer responses at 100 μA (30 vs. 100 μA: excit.: NAc_{Med}: p = 0.05; NAc_{Core}: p = 0.26). Further increasing stimulation intensity from 100 μA to 300 μA significantly increased the proportions of excitatory responses in both subregions (100 vs. 300 μA: excit.: NAc_{Med}: p = 0.0; NAc_{Core}: p = 0.004). By contrast, for inhibitory responses a 30-to-100 μA stimulus intensity change was sufficient to significantly increase their prevalence in both NAc_{Med} and NAc_{Core} (30 vs. 100 μA: inh.: NAc_{Med}: p = 0.04; NAc_{Core}: p = 0.0). Further increase to 300 μA did not significantly affect inhibitory response prevalence in either subregion (100 vs. 300 μA: inh.: NAc_{Med}: p = 0.27; NAc_{Core}: p = 0.29). Notably, the localized nature of DCN stimulation was not compromised at 300 μA (comparison to marginal probability at 100 μm from most effective DCN site: p = 0.2; Table 2J-K). Collectively, these results suggest that DCN stimulation more effectively (i.e., at lower intensities) modulates inhibitory responses than excitatory ones, with NAc_{Med} being more responsive than NAc_{Core}. Modulation of excitatory responses requires stronger inputs, and this is particularly applicable to NAc_{Med}.

Response onset latencies are largely unaffected by DCN stimulation intensity

To investigate effects of DCN input strength on temporal characteristics of NAc responses, we examined the dependence of response onset latencies on DCN stimulation intensity. After correction for multiple comparisons, we found that increasing stimulation intensity did not significantly affect onset latencies of either excitatory or inhibitory responses, in either NAc_{Med} or NAc_{Core} (Table 2G-I). In agreement with our previous results (Fig. 3C), we found that, overall, excitatory responses tended to be faster than inhibitory ones. This is apparent in the 3-D color plots of z-transformed spiking activity for inhibitory and excitatory

bioRxiv preprint doi: https://doi.org/10.1101/2020.09.28.283952; this version posted September 29, 2020. The copyright holder for this preprint (which was not certified by peer review) is the author/funder. All rights reserved. No reuse allowed without permission.

responders (Fig. 5B) (see Fig. 5S1 for non-responders), as well as the frequency histograms of threshold crossings across all recorded sites (Fig. 5S2). Further quantification indicated that excitatory responses of NAc_{Med} had significantly shorter onset latencies than inhibitory ones at 300-µA stimulation [onset latency (in s): mean ± SEM: NAc_{Med}: 300 µA: excit. 0.32 ± 0.17, inh.: 1.24 ± 0.20, p = 0.0]. The 100-µA dataset did not reach significant difference (p = 0.25), probably due to sample size differences. In NAc_{Core}, excitatory responses were faster than inhibitory ones at 100-µA and 300-µA stimulation [onset latency (in s): NAc_{Core}: 100 µA: excit. 0.11 ± 0.03, inh.: 1.08 ± 0.14, p = 0.0; 300 µA: excit. 0.32 ± 0.15, inh.: 1.29 ± 0.18, p = 0.0] (Fig. 5D) (Table 2G,H). Comparing between subregions, our previous observation that excitatory responses in NAc_{Core} were faster than in NAc_{Med} (Table 1G) was also confirmed here (100 µA: p = 0.03). There was no significant difference between the two subregions in the onset latencies of excitatory responses evoked by 30-µA or 300-µA stimulation (excit.: NAc_{Med} vs. NAc_{Core}: 30 µA: p = 0.06; 300 µA: p = 0.57); or in the latencies of inhibitory responses evoked by any stimulation intensity (inh.: NAc_{Med} vs. NAc_{Core}: 30 µA: p = 0.98; 100 µA: p = 0.18; 300 µA: p = 0.59). The overall picture emerging from these analyses points to NAc receiving fast excitatory and slow inhibitory inputs in response to DCN stimulation. NAc_{Med} appears more attuned to inhibitory inputs, with significant excitation recruited only with very strong stimulation, whereas NAc_{Core} receives faster and more prevalent excitation compared to NAc_{Med}.

Anatomical blueprint of CB-NAc connectivity

There are no direct, monosynaptic connections between CB and NAc (Allen Brain Atlas, and our own observations); we therefore hypothesized the existence of at least disynaptic anatomical pathways between the two regions. To test this hypothesis, we adopted a 2-prong approach. First, we combined injection of a retrograde tracer (cholera toxin subunit B (ctb) -640 or -568) in NAc with injection of an anterograde viral tracer (AAV9-CAG-GFP) in DCN to identify areas of overlap (nodes) in a putative disynaptic CB-NAc circuit (Fig. 6A,B). Histological processing and confocal imaging of brain sections (n = 3 mice with successful NAc and DCN injections, without spill to neighboring regions) revealed two regions of overlap between ctb-filled neurons that project to NAc and GFP-labelled DCN axonal projections: the VTA and limbic thalamus (Fig. 6C,D). In VTA, most areas of overlap localized medially and caudally and involved both TH+ (dopaminergic) neurons and TH- neurons (Fig. 6C). In

bioRxiv preprint doi: https://doi.org/10.1101/2020.09.28.283952; this version posted September 29, 2020. The copyright holder for this preprint (which was not certified by peer review) is the author/funder. All rights reserved. No reuse allowed without permission.

thalamus, we found areas of overlap in parafascicular (PF) and anterior centromedial (CM) intralaminar nuclei (Fig. 6D). These results are consistent with the existence of a disynaptic CB-NAc anatomical circuit, and point to VTA and intralaminar thalamic nuclei as putative nodes.

To independently confirm these observations, we performed AAV1-mediated anterograde transsynaptic tracing experiments[67] via stereotactic injections of AAV1-Cre in DCN and AAV-FLEX-tdTomato in VTA or limbic thalamus (Fig. 7A,B). The approach relies on the transsynaptic transfer of Cre to postsynaptic neurons, which -once infected with a floxed fluorophore- will become fluorescently labeled. With this method, we confirmed the existence of neurons receiving CB input in VTA (Fig. 7C1,C2) and limbic thalamus (Fig. 7E1,E2). Importantly, we were able to localize their labeled axonal projections in NAc, in both NAc_{Med} and NAc_{Core} (Fig. 7D,F). Similar projection patterns were observed when AAV1-Cre was injected in lateral DCN only (not shown). These findings chart the blueprint of disynaptic CB-NAc connectivity and provide an anatomical foundation for our newly discovered CB-NAc functional connection.

Discussion

In this study we examined the uncharted functional connectivity between CB and NAc through in vivo electrophysiology. We found that electrical microstimulation of DCN modulates spiking activity in NAc and elicits responses in both NAc_{Med} and NAc_{Core}. In both subregions, these responses manifested as inhibitory and/or excitatory modulations of spiking activity and exhibited NAc subregion-specificity with respect to response-type prevalence, latency, and dependence on stimulus intensity.

First, we found that weak-to-moderate DCN stimulation reliably evoked inhibitory, but not excitatory, responses in NAc_{Med}. Excitatory responses in NAc_{Med} could be reliably evoked only with the strongest DCN stimulation. In contrast, even moderate stimulation could reliably induce both inhibitory and excitatory responses in NAc_{Core}. Second, we found differences between the two subregions with respect to onset latency: excitatory responses were faster to start and shorter-lasting than inhibitory ones in both subregions. In NAc_{Core} in particular, excitatory responses tended to be faster than in NAc_{Med}. The differences in response profiles

bioRxiv preprint doi: https://doi.org/10.1101/2020.09.28.283952; this version posted September 29, 2020. The copyright holder for this preprint (which was not certified by peer review) is the author/funder. All rights reserved. No reuse allowed without permission.

between NAc_{Med} and NAc_{Core} are consistent with the fact that the anatomy and functions of these NAc subregions also differ[55,60,61,63,68,69].

The differences in prevalence, temporal characteristics and induction threshold of responses between NAc_{Med} and NAc_{Core} suggest that the two subregions do not receive the same copy of the CB signal. These differences are unlikely to arise from within DCN, because our analyses of the topographical organization of effective DCN stimulation sites (Fig. 4) indicated widespread and overlapping distributions of sites that could evoke excitatory or inhibitory responses in NAc_{Med} and/or NAc_{Core}. Even sites as close as 100 μm from each other could evoke quite different responses. If these different response profiles in NAc arise from distinct sources within DCN, these sources are likely organized at a scale below the resolution of our study (e.g., at the cellular level). Moreover, even if distinct pools of DCN neurons transmit signals to the two NAc subregions, the onset latency differential between responses suggests at least some divergence in the downstream routes that DCN signals take to arrive at their NAc destinations.

The CB's influence on NAc spiking activity is probably served by disynaptic (and/or possibly polysynaptic) pathways. This is supported by the finding that the onset of both excitatory and inhibitory responses in NAc_{Med}, as well as the onset of at least the inhibitory responses in NAc_{Core}, occurred well past the onset of stimulation and its artifact, which placed a lower bound on the latencies we were able to detect confidently. Our electrophysiological observations are also consistent with tracing experiments (Allen Brain Atlas; our own preliminary work) that have not found direct anatomical connections between CB and NAc, and are further corroborated by our viral tracing experiments (Figs. 6,7), which point to VTA and intralaminar nuclei as nodes in CB-NAc communication routes.

Anatomical and functional connections between DCN and VTA, and DCN and intralaminar n. nodes, have been described previously[20,44,70–73]. VTA and thalamic projections to NAc are also well established[62,74–81]. It might therefore not be surprising that the CB recruits these nodes to communicate with NAc. However, the VTA and thalamus are exquisitely complex areas with multiple output streams. For example, the VTA projects not only to NAc but also to hippocampus, hypothalamus, lateral habenula, entorhinal cortex, etc.[82–84]. None of these downstream target regions appears to be disynaptically connected to DCN, which points

bioRxiv preprint doi: https://doi.org/10.1101/2020.09.28.283952; this version posted September 29, 2020. The copyright holder for this preprint (which was not certified by peer review) is the author/funder. All rights reserved. No reuse allowed without permission.

to specificity in circuit wiring. Our study is the first one, to our knowledge, to map a CB-VTA-NAc circuit. A very recent study provided anatomical evidence for a disynaptic medial DCN-NAc circuit[43]. Here we extend these observations to lateral DCN and also provide evidence for the centromedial and parafascicular nuclei as parts of the thalamic node.

The cell types and properties of nodal neurons that receive DCN input remain incompletely understood. In the VTA, for example, glutamatergic DCN projections target both dopaminergic and non-dopaminergic neurons[20,73,85]. Given the known heterogeneity of VTA neural populations[86,87], DCN inputs could activate dopaminergic, GABAergic, glutamatergic, and/or dual neurotransmitter-releasing neurons. This diversity in neural types, which are known to project to NAc with some subregion-specificity[57,81,88–92], could at least partly explain the differences in responses and onset latencies we observed in our experiments. For example, dopamine's action on G protein-coupled receptors to modulate neuronal activity could be responsible for the long latencies and/or duration in NAc_{Med} inhibitory responses. Thalamic neurons also show at least partial NAc subregion specificity[61,74,93], which could explain the faster excitatory responses in NAc_{Core} compared to NAc_{Med}.

It is tempting to speculate on network-wide implications of the different CB-NAc response profiles. The fast excitatory profiles would be well poised to support the rapid communication of information critical to the control of motivated behavior, such as prediction or prediction-error signals, which are well established in the cerebellum[19,21,22,94]. The slower, less synchronous and longer-lasting inputs may be suggestive of a regulatory function, e.g. gain control of the communication between NAc and other brain regions (Buzsáki et al., 2007). If the DCN signals do in fact reach NAc_{Med} and NAc_{Core} through distinct pathways, this leaves room for their distinct multiplexing with signals originating elsewhere. Future investigations into the cellular basis of CB-NAc communication as well as its behavioral contributions are clearly in order. Here, we have broken new ground by providing the first evidence of functional connectivity between CB and NAc, identifying its NAc subregion-dependence, and offering an anatomical blueprint that could serve as its foundation.

bioRxiv preprint doi: https://doi.org/10.1101/2020.09.28.283952; this version posted September 29, 2020. The copyright holder for this preprint (which was not certified by peer review) is the author/funder. All rights reserved. No reuse allowed without permission.

Conflict of Interest

The authors declare that the research was conducted in the absence of any commercial or financial relationships that could be construed as a potential conflict of interest.

Author contribution

AD, EA and DF designed the research; AD and SJJ performed the research; AD and EA analyzed the data; SG assisted with tissue slicing and registration; SJJ assisted with preparation of anatomy figures; AD, EA and DF wrote the paper.

Funding

This work was supported by a Whitehall fellowship, BRFSG-2017-02, R21MH114178 and NSF1754831 to DF; a NARSAD 2018 Young Investigator Award to EA; AD was supported by NIH Grant T32 GM 007377 and a UC Davis Dean's Distinguished Graduate Fellowship.

Figure legends

Figure 1. Cerebellar stimulation elicits excitatory and inhibitory responses in NAc. A, Schematic diagram of recording setup. Recording electrode array was lowered into NAc and bipolar stimulating electrode was lowered into deep cerebellar nuclei. Stimulation protocol consisted of 10 trials (inter-trial interval: 15 s) of five 100 µA, 0.5-ms pulses at 200 Hz. **B**, Recording sites in NAc_{Med} and NAc_{Core}. Numbers at bottom of slices indicate distance from bregma. **C**-**D**, Examples of inhibitory and excitatory responses in NAc_{Med} (C) and NAc_{Core} (D), respectively, as a function of time. *Top,* 4-s raster plots of spiking activity; *Middle*, Peri-stimulus time histograms of firing rate (10-ms bin); *Bottom*, Average firing rate, normalized to baseline (z-score). Red dotted lines indicate response threshold, set at -3.2 for inhibitory responses and +4.0 for excitatory responses. Stimulus artifacts have been masked for clarity (teal bars).

Figure 2. The distribution of response types differs between NAc shell and core. A, Percent of recordings crossing positive (*blue*) or negative (*red*) threshold at each 10-ms time bin for NAc_{Med} (A1) and NAc_{Core} (A2) regions, as a function of time. Shaded area indicates 3-s response window. **B**, Pie charts of distribution of response types in NAc_{Med} and NAc_{Core}. Recordings that cross positive threshold within the response window are classified as excitatory

bioRxiv preprint doi: https://doi.org/10.1101/2020.09.28.283952; this version posted September 29, 2020. The copyright holder for this preprint (which was not certified by peer review) is the author/funder. All rights reserved. No reuse allowed without permission.

responders (*blue*); recordings that cross negative threshold: inhibitory (*red*); recordings that do not cross either threshold: non-responders (*gray*). **C**, Comparison of % responses vs. pre-stimulus baseline, by type (excitatory, inhibitory) and NAc region (shell, core). * $p < 0.05$, corrected for multiple comparisons (FDR 10%).

Figure 2- figure supplement 1. Robustness of response distributions to small fluctuations in threshold. Percent threshold crossings during response window (solid lines) and pre-stimulus baseline (dotted lines) for different types of responses (*red*: inhibitory; *blue*: excitatory) in NAc_{Med} and NAc_{Core}, as a function of threshold. Selected threshold values (vertical dashed line) maintain a maximum of 5% crossings during baseline (horizontal dashed line) for each response type and NAc subregion. **B**, Same as in A, but for subset of data that compared three CB stimulation intensities (30, 100 and 300 µA).

Figure 3. Excitatory and inhibitory responses show different temporal profiles. A,**B**, Heat maps of firing rate (z-score) of excitatory (A) and inhibitory (B) responders in NAc shell and core, as a function of time. Responders were ordered on the y-axis by response onset latency. Black triangle denotes time of stimulation; white vertical bars mask stimulus artifact for clarity. **C**, Comparison of onset latencies for excitatory and inhibitory responses within each NAc subregion. * $p < 0.05$, corrected for multiple comparisons (FDR 10%). **D1**,**D2**, Cumulative probability histograms of threshold crossings for excitatory (D1) and inhibitory (D2) responders in NAc shell and core, with most crossings falling within 3 seconds of stimulus onset (shaded region).

Figure 3- figure supplement 1. Heat maps of non-responders at 100 µA stimulation. Firing rate (z-score) of non-responders, ordered on the y-axis by latency of peak response amplitude, as a function of time. Gray box outlines the response window.

Figure 4. Differential distribution of excitatory and inhibitory responses in NAc is not due to topographical specialization within CB. A, The lateral or interposed DCN was electrically stimulated. Abbreviations: m: medial n., ip: interposed n.; lat: lateral n. **B**,**C**, Stereotactic coordinates of CB stimulation sites in ML-DV (B1,C1), ML-AP (B2,C2), and AP-DV (B3,C3)

bioRxiv preprint doi: https://doi.org/10.1101/2020.09.28.283952; this version posted September 29, 2020. The copyright holder for this preprint (which was not certified by peer review) is the author/funder. All rights reserved. No reuse allowed without permission.

planes. Colored dots denote sites that evoked excitatory (*blue*), inhibitory (*red*), or no responses (*gray*) in NAc_{Med} (B) and NAc_{Core} (C). Abbreviations: ML: medio-lateral, DV: dorso-ventral, AP: antero-posterior, excit.: excitatory, inh.: inhibitory, non-resp.: non-responding. **D**, Spatial resolution of stimulation (current spread). Plot of the probability that a stimulation site would elicit a NAc response at various distances from the CB site that elicited the strongest response in each experiment (most effective site at distance d = 0 µm). Black horizontal line shows marginal response probability.

Figure 5. Varying CB stimulation intensity changes the relative distribution of response types within NAc, but leaves temporal profiles mostly unaffected. A, Distribution of response types in NAc shell (A1) and core (A2) evoked by 30 µA, 100 µA and 300 µA bipolar CB stimulation. **B**, Comparison of % responses vs. pre-stimulus baseline, by type (excitatory, inhibitory), stimulation intensity (30 µA, 100 µA and 300 µA), and NAc subregion (shell, core). * $p < 0.05$, corrected for multiple comparisons (FDR 10%)(see also Table 2). **C**, Firing rate (z-score) heat maps of excitatory and inhibitory responders in NAc shell and core, as a function of time. Responders were ordered on the y-axis by latency of response onset. Black triangle denotes time of stimulation; white vertical bars mask stimulus artifacts for clarity. **D**, Boxplots of onset latencies for excitatory and inhibitory responses in NAc shell (*top*) and core (*bottom*), elicited by 30 µA, 100 µA and 300 µA CB stimulation. Figure legend in A also applies to panels B and D. Abbreviations: non-resp.: non-responding, inh.: inhibitory, excit.: excitatory.

Figure 5- figure supplement 1. Profiles of NAc population activity at different CB stimulation intensities. A,B, Time histograms of % recordings in NAc shell (A) and core (B) that cross positive (*blue*) or negative (*red*) threshold at each 10-ms time bin, for CB stimulation intensity of 30 µA (A1,B1), 100 µA (A2,B2) and 300 (A3,B3) µA. Shaded region designates 3-s response window.

Figure 6. **Co-localization of NAc-projecting neurons with DCN projections in VTA and intralaminar thalamus**. **A**, Schematic diagrams of stereotactic injections in DCN and NAc. **B1**, Expression of GFP at DCN injection sites. **B2**, Ctb-568 injection site in NAc. **C**, Overlap of ctb-labeled NAc projectors and DCN axons in VTA. **C1**, VTA identification through TH

bioRxiv preprint doi: https://doi.org/10.1101/2020.09.28.283952; this version posted September 29, 2020. The copyright holder for this preprint (which was not certified by peer review) is the author/funder. All rights reserved. No reuse allowed without permission.

immunostaining. **C2**, TH+ neurons. **C3**, Ctb-labeled NAc projectors. **C4**, GFP-expressing DCN axons. **C5**, C2-C4 merged. **D**, Overlap of ctb-labeled NAc projectors (red) and GFP-expressing DCN axons (green) in intralaminar thalamic nuclei. **D1**-**D2**, Overlap in parafascicular n. **D3**-**D4**, Overlap in centromedial n. Yellow boxes in C1,D1,D3 denote zoom-in areas depicted in C2-C5, D2 and D4, respectively. Scale bars: B1-2,C1,D1,D3: 200 µm; C2-C5: 20 µm; D2,D4: 10 µm. Blue: DAPI. Numbers denote distance from bregma.

Figure 7. **Disynaptic CB-NAc connectivity is confirmed via anterograde transsynaptic viral tracing**. **A**, Schematic diagram of AAV1-mediated transsynaptic labeling approach. **B**, Schematic diagrams of stereotactic injections of floxed fluorophore in VTA and thalamic nodes. **C1**, The VTA is visualized via TH immunostaining (green). Yellow box denotes zoom-in area depicted in C2. Rn: red nucleus; ml: medial lemniscus. **C2**, Neurons that receive DCN input are labeled with tdTomato. Green: TH+ neurons (arrow). Red: tdTomato+ neurons (white arrowhead). Orange: TH+, tdTomato+ neuron (yellow arrowhead). **D**, Projections of CB-VTA neurons in NAc shell (NAc_{Med}) and core (NAc_{Core}). **E1**, Neurons that receive DCN input in thalamus are labeled with tdTomato (red). Blue: NeuN. CM: centromedial n.; PC: paracentral n.; CL: centrolateral n.; VL: ventrolateral n. **D2**, Same as D1, but for parafascicular n. (PF). fr: fasciculus retroflexus. **F**, Projections of CB-thalamic neurons in NAc_{Med} and in NAc_{Core}. Scale bars below images: 500 µm, except for C2: 100 µm. Numbers denote distance from bregma.

bioRxiv preprint doi: https://doi.org/10.1101/2020.09.28.283952; this version posted September 29, 2020. The copyright holder for this preprint (which was not certified by peer review) is the author/funder. All rights reserved. No reuse allowed without permission.

References

1. Ito, M. Cerebellar circuitry as a neuronal machine. *Prog. Neurobiol.* **78**, 272–303 (2006).
2. Buckner, R. L. The cerebellum and cognitive function: 25 years of insight from anatomy and neuroimaging. *Neuron* **80**, 807–815 (2013).
3. Hull, C. Prediction signals in the cerebellum: beyond supervised motor learning. *eLife* **9**, (2020).
4. Liang, K. J. & Carlson, E. S. Resistance, vulnerability and resilience: A review of the cognitive cerebellum in aging and neurodegenerative diseases. *Neurobiology of Learning and Memory* (2019) doi:10.1016/j.nlm.2019.01.004.
5. Sokolov, A. A., Miall, R. C. & Ivry, R. B. The Cerebellum: Adaptive Prediction for Movement and Cognition. *Trends in Cognitive Sciences* **21**, 313–332 (2017).
6. Guo, Z. *et al.* Brain areas activated by uncertain reward-based decision-making in healthy volunteers. *Neural Regen Res* **8**, 3344–3352 (2013).
7. Ernst, M. Decision-making in a Risk-taking Task A PET Study. *Neuropsychopharmacology* **26**, 682–691 (2002).
8. Moulton, E. A., Elman, I., Becerra, L. R., Goldstein, R. Z. & Borsook, D. The cerebellum and addiction: insights gained from neuroimaging research. *Addict Biol* **19**, 317–331 (2014).
9. Ernst, T. M. *et al.* The cerebellum is involved in processing of predictions and prediction errors in a fear conditioning paradigm. *eLife* **8**, (2019).
10. Wang, S. S.-H., Kloth, A. D. & Badura, A. The cerebellum, sensitive periods, and autism. *Neuron* **83**, 518–532 (2014).
11. D'Mello, A. M. & Stoodley, C. J. Cerebro-cerebellar circuits in autism spectrum disorder. *Frontiers in Neuroscience* **9**, (2015).
12. Sathyanesan, A. *et al.* Emerging connections between cerebellar development, behaviour and complex brain disorders. *Nature Reviews Neuroscience* **20**, 298–313 (2019).
13. Rabellino, D., Densmore, M., Théberge, J., McKinnon, M. C. & Lanius, R. A. The cerebellum after trauma: Resting-state functional connectivity of the cerebellum in posttraumatic stress disorder and its dissociative subtype. *Human Brain Mapping* **39**, 3354–3374 (2018).
14. Lanius, R. A. *et al.* The innate alarm system in PTSD: conscious and subconscious processing of threat. *Current Opinion in Psychology* **14**, 109–115 (2017).
15. Roy, A. K. *et al.* Intrinsic functional connectivity of amygdala-based networks in adolescent generalized anxiety disorder. *J Am Acad Child Adolesc Psychiatry* **52**, 290-299.e2 (2013).
16. Schmahmann, J. D. The cerebellum and cognition. *Neuroscience Letters* **688**, 62–75 (2019).
17. Miquel, M. *et al.* Have we been ignoring the elephant in the room? Seven arguments for considering the cerebellum as part of addiction circuitry. *Neuroscience & Biobehavioral Reviews* **60**, 1–11 (2016).
18. Volkow, N. D., Wang, G.-J., Tomasi, D. & Baler, R. D. Unbalanced neuronal circuits in addiction. *Current Opinion in Neurobiology* **23**, 639–648 (2013).
19. Wagner, M. J., Kim, T. H., Savall, J., Schnitzer, M. J. & Luo, L. Cerebellar granule cells encode the expectation of reward. *Nature* (2017) doi:10.1038/nature21726.
20. Carta, I., Chen, C. H., Schott, A. L., Dorizan, S. & Khodakhah, K. Cerebellar modulation of the reward circuitry and social behavior. *Science* **363**, eaav0581 (2019).

bioRxiv preprint doi: https://doi.org/10.1101/2020.09.28.283952; this version posted September 29, 2020. The copyright holder for this preprint (which was not certified by peer review) is the author/funder. All rights reserved. No reuse allowed without permission.

21. Kostadinov, D., Beau, M., Pozo, M. B. & Häusser, M. Predictive and reactive reward signals conveyed by climbing fiber inputs to cerebellar Purkinje cells. *Nature Neuroscience* **22**, 950–962 (2019).
22. Heffley, W. & Hull, C. Classical conditioning drives learned reward prediction signals in climbing fibers across the lateral cerebellum. *eLife* **8**, (2019).
23. Ma, M. *et al.* Molecular layer interneurons in the cerebellum encode for valence in associative learning. *Nature Communications* **11**, (2020).
24. Otsuka, S. *et al.* Roles of Cbln1 in Non-Motor Functions of Mice. *J. Neurosci.* **36**, 11801–11816 (2016).
25. Strata, P. The Emotional Cerebellum. *Cerebellum* (2015) doi:10.1007/s12311-015-0649-9.
26. Adamaszek, M. *et al.* Consensus Paper: Cerebellum and Emotion. *The Cerebellum* **16**, 552–576 (2017).
27. Supple, W. F., Jr, Leaton, R. N. & Fanselow, M. S. Effects of cerebellar vermal lesions on species-specific fear responses, neophobia, and taste-aversion learning in rats. *Physiol. Behav.* **39**, 579–586 (1987).
28. Jackman, S. L. *et al.* Cerebellar Purkinje cell activity modulates aggressive behavior. *eLife* **9**, (2020).
29. Sacchetti, B., Baldi, E., Lorenzini, C. A. & Bucherelli, C. Cerebellar role in fear-conditioning consolidation. *Proc. Natl. Acad. Sci. U.S.A.* **99**, 8406–8411 (2002).
30. Lorivel, T., Roy, V. & Hilber, P. Fear-related behaviors in Lurcher mutant mice exposed to a predator. *Genes Brain Behav.* **13**, 794–801 (2014).
31. Bauer, D. J., Kerr, A. L. & Swain, R. A. Cerebellar dentate nuclei lesions reduce motivation in appetitive operant conditioning and open field exploration. *Neurobiology of Learning and Memory* **95**, 166–175 (2011).
32. Caston, J., Chianale, C., Delhaye-Bouchaud, N. & Mariani, J. Role of the cerebellum in exploration behavior. *Brain Res.* **808**, 232–237 (1998).
33. Peterson, T. C. *et al.* Behavior modification after inactivation of cerebellar dentate nuclei. *Behavioral Neuroscience* **126**, 551–562 (2012).
34. Xiao, L. & Scheiffele, P. Local and long-range circuit elements for cerebellar function. *Current Opinion in Neurobiology* **48**, 146–152 (2018).
35. Reeber, S. L., Otis, T. S. & Sillitoe, R. V. New roles for the cerebellum in health and disease. *Frontiers in Systems Neuroscience* **7**, (2013).
36. Ito, M. Control of mental activities by internal models in the cerebellum. *Nature Reviews Neuroscience* **9**, 304–313 (2008).
37. Watson, T. C., Becker, N., Apps, R. & Jones, M. W. Back to front: cerebellar connections and interactions with the prefrontal cortex. *Frontiers in Systems Neuroscience* **8**, (2014).
38. Mittleman, G., Goldowitz, D., Heck, D. H. & Blaha, C. D. Cerebellar modulation of frontal cortex dopamine efflux in mice: relevance to autism and schizophrenia. *Synapse* **62**, 544–550 (2008).
39. Gao, Z. *et al.* A cortico-cerebellar loop for motor planning. *Nature* **563**, 113–116 (2018).
40. Kelly, E. *et al.* Regulation of autism-relevant behaviors by cerebellar–prefrontal cortical circuits. *Nature Neuroscience* (2020) doi:10.1038/s41593-020-0665-z.
41. Brady, R. O. *et al.* Cerebellar-Prefrontal Network Connectivity and Negative Symptoms in Schizophrenia. *American Journal of Psychiatry* **176**, 512–520 (2019).
42. Strick, P. L., Dum, R. P. & Fiez, J. A. Cerebellum and Nonmotor Function. *Annual Review of Neuroscience* **32**, 413–434 (2009).

bioRxiv preprint doi: https://doi.org/10.1101/2020.09.28.283952; this version posted September 29, 2020. The copyright holder for this preprint (which was not certified by peer review) is the author/funder. All rights reserved. No reuse allowed without permission.

43. Fujita, H., Kodama, T. & du Lac, S. Modular output circuits of the fastigial nucleus for diverse motor and nonmotor functions of the cerebellar vermis. *eLife* **9**, e58613 (2020).
44. Snider, R. S. & Maiti, A. Cerebellar contributions to the Papez circuit. *J. Neurosci. Res.* **2**, 133–146 (1976).
45. Zeidler, Z., Hoffmann, K. & Krook-Magnuson, E. HippoBellum: acute cerebellar modulation alters hippocampal dynamics and function. *The Journal of Neuroscience* JN-RM-0763-20 (2020) doi:10.1523/JNEUROSCI.0763-20.2020.
46. Dietrichs, E. & Haines, D. E. Interconnections between hypothalamus and cerebellum. *Anatomy and Embryology* **179**, 207–220 (1989).
47. Heath, R. G., Dempesy, C. W., Fontana, C. J. & Myers, W. A. Cerebellar stimulation: effects on septal region, hippocampus, and amygdala of cats and rats. *Biol. Psychiatry* **13**, 501–529 (1978).
48. Rochefort, C. *et al.* Cerebellum Shapes Hippocampal Spatial Code. *Science* **334**, 385–389 (2011).
49. Floresco, S. B. The Nucleus Accumbens: An Interface Between Cognition, Emotion, and Action. *Annual Review of Psychology* **66**, 25–52 (2015).
50. Klawonn, A. M. & Malenka, R. C. Nucleus Accumbens Modulation in Reward and Aversion. *Cold Spring Harbor Symposia on Quantitative Biology* **83**, 119–129 (2018).
51. Holtzman-Assif, O., Laurent, V. & Westbrook, R. F. Blockade of dopamine activity in the nucleus accumbens impairs learning extinction of conditioned fear. *Learn. Mem.* **17**, 71–75 (2010).
52. Albert, T. J., Dempesy, C. W. & Sorenson, C. A. Anterior cerebellar vermal stimulation: Effect on behavior and basal forebrain neurochemistry in rat. *Biological Psychiatry* **20**, 1267–1276 (1985).
53. Holloway, Z. R. *et al.* Cerebellar Modulation of Mesolimbic Dopamine Transmission Is Functionally Asymmetrical. *The Cerebellum* **18**, 922–931 (2019).
54. Dempesy, C. W. *et al.* Stimulation of the paleocerebellar cortex of the cat: increased rate of synthesis and release of catecholamines at limbic sites. *Biol. Psychiatry* **18**, 127–132 (1983).
55. Luo, R. *et al.* A dopaminergic switch for fear to safety transitions. *Nature Communications* **9**, (2018).
56. Zell, V. *et al.* VTA Glutamate Neuron Activity Drives Positive Reinforcement Absent Dopamine Co-release. *Neuron* **107**, 864-873.e4 (2020).
57. Root, D. H. *et al.* Distinct Signaling by Ventral Tegmental Area Glutamate, GABA, and Combinatorial Glutamate-GABA Neurons in Motivated Behavior. *Cell Reports* **32**, 108094 (2020).
58. Zahm, D. S. Functional-anatomical Implications of the Nucleus Accumbens Core and Shell Subterritories. *Annals of the New York Academy of Sciences* **877**, 113–128 (1999).
59. Corbit, L. H. & Balleine, B. W. The General and Outcome-Specific Forms of Pavlovian-Instrumental Transfer Are Differentially Mediated by the Nucleus Accumbens Core and Shell. *Journal of Neuroscience* **31**, 11786–11794 (2011).
60. Ito, R. & Hayen, A. Opposing Roles of Nucleus Accumbens Core and Shell Dopamine in the Modulation of Limbic Information Processing. *Journal of Neuroscience* **31**, 6001–6007 (2011).
61. Li, Z. *et al.* Cell-Type-Specific Afferent Innervation of the Nucleus Accumbens Core and Shell. *Frontiers in Neuroanatomy* **12**, (2018).

bioRxiv preprint doi: https://doi.org/10.1101/2020.09.28.283952; this version posted September 29, 2020. The copyright holder for this preprint (which was not certified by peer review) is the author/funder. All rights reserved. No reuse allowed without permission.

62. Groenewegen, H. J., Wright, C. I., Beijer, A. V. & Voorn, P. Convergence and segregation of ventral striatal inputs and outputs. *Ann. N. Y. Acad. Sci.* **877**, 49–63 (1999).
63. Badrinarayan, A. *et al.* Aversive Stimuli Differentially Modulate Real-Time Dopamine Transmission Dynamics within the Nucleus Accumbens Core and Shell. *Journal of Neuroscience* **32**, 15779–15790 (2012).
64. Oden, A. & Wedel, H. Arguments for Fisher's Permutation Test. *Ann. Statist.* **3**, 518–520 (1975).
65. Antzoulatos, E. G. & Miller, E. K. Differences between Neural Activity in Prefrontal Cortex and Striatum during Learning of Novel Abstract Categories. *Neuron* **71**, 243–249 (2011).
66. Benjamini, Y. & Hochberg, Y. Controlling the False Discovery Rate: A Practical and Powerful Approach to Multiple Testing. *Journal of the Royal Statistical Society: Series B (Methodological)* **57**, 289–300 (1995).
67. Zingg, B. *et al.* AAV-Mediated Anterograde Transsynaptic Tagging: Mapping Corticocollicular Input-Defined Neural Pathways for Defense Behaviors. *Neuron* **93**, 33–47 (2017).
68. Floresco, S. B., Montes, D. R., Tse, M. M. T. & van Holstein, M. Differential Contributions of Nucleus Accumbens Subregions to Cue-Guided Risk/Reward Decision Making and Implementation of Conditional Rules. *The Journal of Neuroscience* **38**, 1901–1914 (2018).
69. Ambroggi, F., Ghazizadeh, A., Nicola, S. M. & Fields, H. L. Roles of Nucleus Accumbens Core and Shell in Incentive-Cue Responding and Behavioral Inhibition. *Journal of Neuroscience* **31**, 6820–6830 (2011).
70. Phillipson, O. T. Afferent projections to the ventral tegmental area of Tsai and interfascicular nucleus: A horseradish peroxidase study in the rat. *The Journal of Comparative Neurology* **187**, 117–143 (1979).
71. Gornati, S. V. *et al.* Differentiating Cerebellar Impact on Thalamic Nuclei. *Cell Rep* **23**, 2690–2704 (2018).
72. Hendry, S. H. C., Jones, E. G. & Graham, J. Thalamic relay nuclei for cerebellar and certain related fiber systems in the cat. *The Journal of Comparative Neurology* **185**, 679–713 (1979).
73. Watabe-Uchida, M., Zhu, L., Ogawa, S. K., Vamanrao, A. & Uchida, N. Whole-Brain Mapping of Direct Inputs to Midbrain Dopamine Neurons. *Neuron* **74**, 858–873 (2012).
74. Van der Werf, Y. D., Witter, M. P. & Groenewegen, H. J. The intralaminar and midline nuclei of the thalamus. Anatomical and functional evidence for participation in processes of arousal and awareness. *Brain Res. Brain Res. Rev.* **39**, 107–140 (2002).
75. Su, H.-S. & Bentivoglio, M. Thalamic midline cell populations projecting to the nucleus accumbens, amygdala, and hippocampus in the rat. *The Journal of Comparative Neurology* **297**, 582–593 (1990).
76. Bentivoglio, M., Balercia, G. & Kruger, L. Chapter 4 The specificity of the nonspecific thalamus: The midline nuclei. in *Progress in Brain Research* vol. 87 53–80 (Elsevier, 1991).
77. Ikemoto, S. Dopamine reward circuitry: Two projection systems from the ventral midbrain to the nucleus accumbens–olfactory tubercle complex. *Brain Research Reviews* **56**, 27–78 (2007).
78. Beckstead, R. M., Domesick, V. B. & Nauta, W. J. H. Efferent connections of the substantia nigra and ventral tegmental area in the rat. *Brain Research* **175**, 191–217 (1979).
79. Bassareo, V. & Di Chiara, G. Differential responsiveness of dopamine transmission to food-stimuli in nucleus accumbens shell/core compartments. *Neuroscience* **89**, 637–641 (1999).

bioRxiv preprint doi: https://doi.org/10.1101/2020.09.28.283952; this version posted September 29, 2020. The copyright holder for this preprint (which was not certified by peer review) is the author/funder. All rights reserved. No reuse allowed without permission.

80. Garris, P. A. *et al.* Dissociation of dopamine release in the nucleus accumbens from intracranial self-stimulation. *Nature* **398**, 67–69 (1999).
81. Taylor, S. R. *et al.* GABAergic and glutamatergic efferents of the mouse ventral tegmental area: Mouse VTA projections. *Journal of Comparative Neurology* **522**, 3308–3334 (2014).
82. Oades, R. D. & Halliday, G. M. Ventral tegmental (A10) system: neurobiology. 1. Anatomy and connectivity. *Brain Res.* **434**, 117–165 (1987).
83. Beier, K. T. *et al.* Circuit Architecture of VTA Dopamine Neurons Revealed by Systematic Input-Output Mapping. *Cell* **162**, 622–634 (2015).
84. Stamatakis, A. M. *et al.* A Unique Population of Ventral Tegmental Area Neurons Inhibits the Lateral Habenula to Promote Reward. *Neuron* **80**, 1039–1053 (2013).
85. Beier, K. T. *et al.* Topological Organization of Ventral Tegmental Area Connectivity Revealed by Viral-Genetic Dissection of Input-Output Relations. *Cell Rep* **26**, 159-167.e6 (2019).
86. Morales, M. & Margolis, E. B. Ventral tegmental area: cellular heterogeneity, connectivity and behaviour. *Nature Reviews Neuroscience* **18**, 73–85 (2017).
87. Nair-Roberts, R. G. *et al.* Stereological estimates of dopaminergic, GABAergic and glutamatergic neurons in the ventral tegmental area, substantia nigra and retrorubral field in the rat. *Neuroscience* **152**, 1024–1031 (2008).
88. Root, D. H., Estrin, D. J. & Morales, M. Aversion or Salience Signaling by Ventral Tegmental Area Glutamate Neurons. *iScience* **2**, 51–62 (2018).
89. Mongia, S. *et al.* The Ventral Tegmental Area has calbindin neurons with the capability to co-release glutamate and dopamine into the nucleus accumbens. *European Journal of Neuroscience* **50**, 3968–3984 (2019).
90. Qi, J. *et al.* VTA glutamatergic inputs to nucleus accumbens drive aversion by acting on GABAergic interneurons. *Nature Neuroscience* **19**, 725–733 (2016).
91. Breton, J. M. *et al.* Relative contributions and mapping of ventral tegmental area dopamine and GABA neurons by projection target in the rat. *Journal of Comparative Neurology* (2018) doi:10.1002/cne.24572.
92. Lammel, S. *et al.* Unique Properties of Mesoprefrontal Neurons within a Dual Mesocorticolimbic Dopamine System. *Neuron* **57**, 760–773 (2008).
93. Vertes, R. P., Hoover, W. B. & Rodriguez, J. J. Projections of the central medial nucleus of the thalamus in the rat: Node in cortical, striatal and limbic forebrain circuitry. *Neuroscience* **219**, 120–136 (2012).
94. Larry, N., Yarkoni, M., Lixenberg, A. & Joshua, M. Cerebellar climbing fibers encode expected reward size. *eLife* **8**, (2019).

bioRxiv preprint doi: https://doi.org/10.1101/2020.09.28.283952; this version posted September 29, 2020. The copyright holder for this preprint (which was not certified by peer review) is the author/funder. All rights reserved. No reuse allowed without permission.

TABLE 1

A *NUMBER OF OBSERVATIONS*

		BASELINE		RESPONSE	
	TOTAL	POSITIVE	NEGATIVE	POSITIVE	NEGATIVE (threshold crossings)
NAc SHELL	132	4 (3.0%)	0 (0%)	8 (6.1%)	22 (16.7%)
Nac CORE	117	3 (2.6%)	4 (3.4%)	16 (13.7%)	20 (17.1%)

B *COMPARISONS OF RELATIVE FREQUENCY OF RESPONSES VS. PRE-STIMULUS BASELINE*

	NAc SHELL		NAc CORE	
	POSITIVE	NEGATIVE	POSITIVE	NEGATIVE
p-value*	0.176	**0.0**	**0.003**	**0.0**

* bold red if significant after FDR correction

C *COMPARISON OF PERCENT RESPONDERS IN CORE VS. SHELL*

NAc SHELL	NAc CORE	p-value
22.727273	30.769231	0.111

D *COMPARISONS OF FREQUENCY OF INHIBITORY VS. EXCITATORY RESPONSES*

	NAc SHELL	NAc CORE
p-value	**0.0**	0.142

E *COMPARISONS OF RESPONSE FREQUENCY IN SHELL VS. CORE*

	EXCITATORY	INHIBITORY
p-value	**0.036**	0.548

F *RESPONSE LATENCIES (sec; mean ± SEM)*

	EXCITATORY	INHIBITORY
NAc SHELL	0.63 ± 0.33	1.24 ± 0.15
NAc CORE	0.12 ± 0.02	1.08 ± 0.14

bioRxiv preprint doi: https://doi.org/10.1101/2020.09.28.283952; this version posted September 29, 2020. The copyright holder for this preprint (which was not certified by peer review) is the author/funder. All rights reserved. No reuse allowed without permission.

TABLE 1-continued								
G	*Random permutation tests on response latencies*							
			p-value					
	Excitatory v Inhibitory		**0.0**					
	E v I in Core		**0.0**					
	E v I in Shell		**0.027**					
	Core v Shell		**0.008**					
	Core v Shell in Excit.		**0.048**					
	Core v Shell in Inhib.		0.22					
H	*RISE TIME CONSTANTS (sec)*							
		EXCITATORY	INHIBITORY	p-value				
	NAc SHELL	0.215	1.795	**0.007**				
	NAc CORE	0.175	1.195	**0.0**				
	p-value	0.357	0.056					
I	*SPATIAL SPREAD OF CURRENT (response conditional probability)*							
			proportion	p-value for comparison to marginal				
	distance from most effective site	100 µm	0.211	0.450				
		200 µm	0.278	0.698				
		300 µm	0.250	0.728				
		400 µm	0.200	0.374				
		marginal	0.255					

bioRxiv preprint doi: https://doi.org/10.1101/2020.09.28.283952; this version posted September 29, 2020. The copyright holder for this preprint (which was not certified by peer review) is the author/funder. All rights reserved. No reuse allowed without permission.

TABLE 2

A *NUMBER OF OBSERVATIONS*

			BASELINE		RESPONSE	
		TOTAL	POSITIVE	NEGATIVE	POSITIVE	NEGATIVE
NAc SHELL	30 µA	67	2 (3.0%)	0 (0%)	7 (10.5%)	5 (7.5%)
	100 µA	95	3 (3.2%)	0 (0%)	3 (3.2%)	15 (15.8%)
	300 µA	84	4 (4.8%)	0 (0%)	16 (19.1%)	11 (13.1%)
Nac CORE	30 µA	69	2 (2.9%)	1 (1.5%)	6 (8.7%)	1 (1.5%)
	100 µA	101	2 (2.0%)	4 (4.0%)	12 (11.9%)	20 (19.8%)
	300 µA	75	1 (1.3%)	3 (4.0%)	18 (24%)	13 (17.3%)

B *COMPARISONS OF RELATIVE FREQUENCY OF RESPONSES VS. PRE-STIMULUS BASELINE*

		NAc SHELL		NAc CORE	
		POSITIVE	NEGATIVE	POSITIVE	NEGATIVE
p-value*	30 µA	0.066	**0.028**	0.14	0.50
	100 µA	0.64	**0.0**	**0.005**	**0.0**
	300 µA	**0.003**	**0.0**	**0.0**	**0.004**

* bold red only if significant after FDR correction

C *COMPARISON OF PERCENT RESPONDERS IN CORE VS. SHELL*

	NAc SHELL	NAc CORE	p-value
30 µA	17.9104478	10.144928	0.15
100 µA	18.9473684	31.683168	**0.028**
300 µA	32.1428571	41.333333	0.13

D *COMPARISONS OF FREQUENCY OF INHIBITORY VS. EXCITATORY RESPONSES*

		NAc SHELL	NAc CORE
p-value	30 µA	0.61	**0.029**
	100 µA	**0.0**	**0.011**
	300 µA	0.38	**0.0**

E *COMPARISONS OF RESPONSE FREQUENCY IN SHELL VS. CORE*

		EXCITATORY	INHIBITORY
p-value	30 µA	0.5	0.11
	100 µA	**0.022**	0.287
	300 µA	0.28	0.285

F *COMPARISONS OF RESPONSE FREQUENCY ACROSS STIMULATION INTENSITY*

	EXCITATORY		INHIBITORY	
	NAc SHELL	NAc CORE	NAc SHELL	NAc CORE
30 µA vs. 100 µA	**0.05**	0.257	**0.037**	**0.0**
100 µA vs. 300 µA	**0.0**	**0.004**	0.268	0.29
30 µA vs. 300 µA	**0.023**	**0.004**	0.12	**0.001**

bioRxiv preprint doi: https://doi.org/10.1101/2020.09.28.283952; this version posted September 29, 2020. The copyright holder for this preprint (which was not certified by peer review) is the author/funder. All rights reserved. No reuse allowed without permission.

TABLE 2- continued

G *RESPONSE LATENCIES (sec; mean ± SEM)*

	NAc SHELL		NAc CORE	
	EXCITATORY	INHIBITORY	EXCITATORY	INHIBITORY
30 µA	1.0 ± 0.29	0.89 ± 0.41	0.41 ± 0.22	2.58 ± 0.0
100 µA	0.88 ± 0.69	1.27 ± 0.20	0.11 ± 0.03	1.08 ± 0.14
300 µA	0.32 ± 0.17	1.24 ± 0.20	0.32 ± 0.15	1.29 ± 0.18

H *Random permutation tests on response latencies*

	p-value		
	30 µA	100 µA	300 µA
Excitatory v Inhibitory	0.13	**0.0**	**0.0**
E v I in Core	0.13	**0.0**	**0.0**
E v I in Shell	0.59	0.25	**0.0**
Core v Shell	0.27	**0.021**	0.55
Core v Shell in Excit.	0.06	**0.029**	0.57
Core v Shell in Inhib.	0.98	0.18	0.59

I

	30vs100 µA	100vs300 µA	30vs300 µA
Core/Excitatory	0.13	0.13	0.24
Core/Inhibitory	0.034	0.16	0.052
Shell/Excitatory	0.44	0.16	0.045
Shell/Inhibitory	0.15	0.44	0.21

J *SPATIAL SPREAD OF CURRENT (responder probability)*

		stimulation intensity		
		30 µA	100 µA	300 µA
distance from most effective site	100 µm	0.13	0.17	0.27
	200 µm	0.06	0.28	0.24
	300 µm	0.0	0.25	0.0
	400 µm	0.0	0.20	0.25
	marginal prob	0.14	0.26	0.37

K *Comparison to marginal (p-values of random permutation test)*

		stimulation intensity		
		30 µA	100 µA	300 µA
distance from most effective site	100 µm	0.662	0.284	0.211
	200 µm	0.094	0.699	0.057
	300 µm	0.637	0.720	0.027
	400 µm	0.371	0.383	0.277

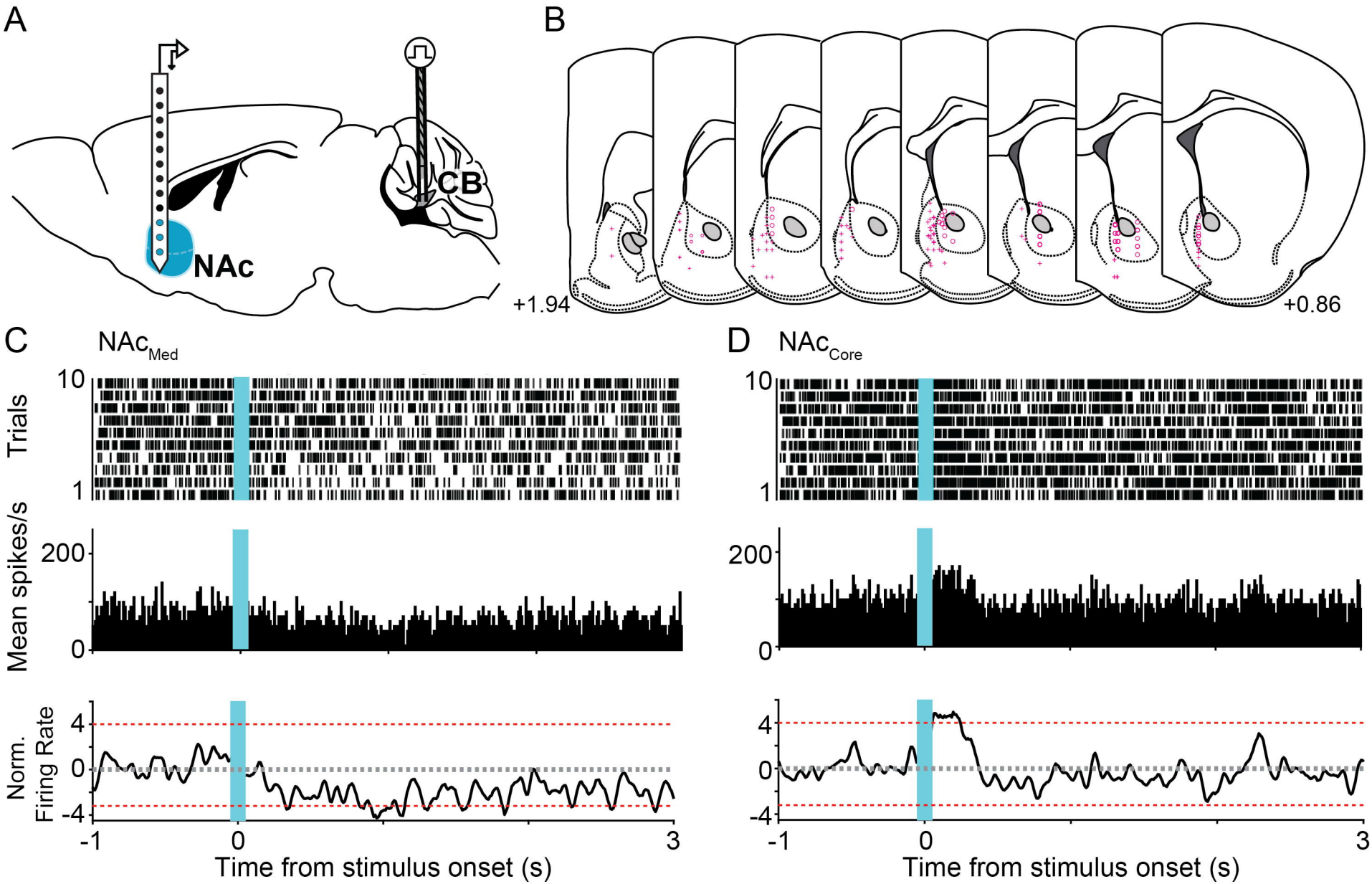
A
NAc
CB
B
+1.94
+0.86
C
NAcMed
D
NAcCore
Trials
10
1
Mean spikes/s
200
0
Norm. Firing Rate
4
0
-4
-1
0
3
Time from stimulus onset (s)

Figure 1

bioRxiv preprint doi: https://doi.org/10.1101/2020.09.28.283952; this version posted September 29, 2020. The copyright holder for this preprint (which was not certified by peer review) is the author/funder. All rights reserved. No reuse allowed without permission.

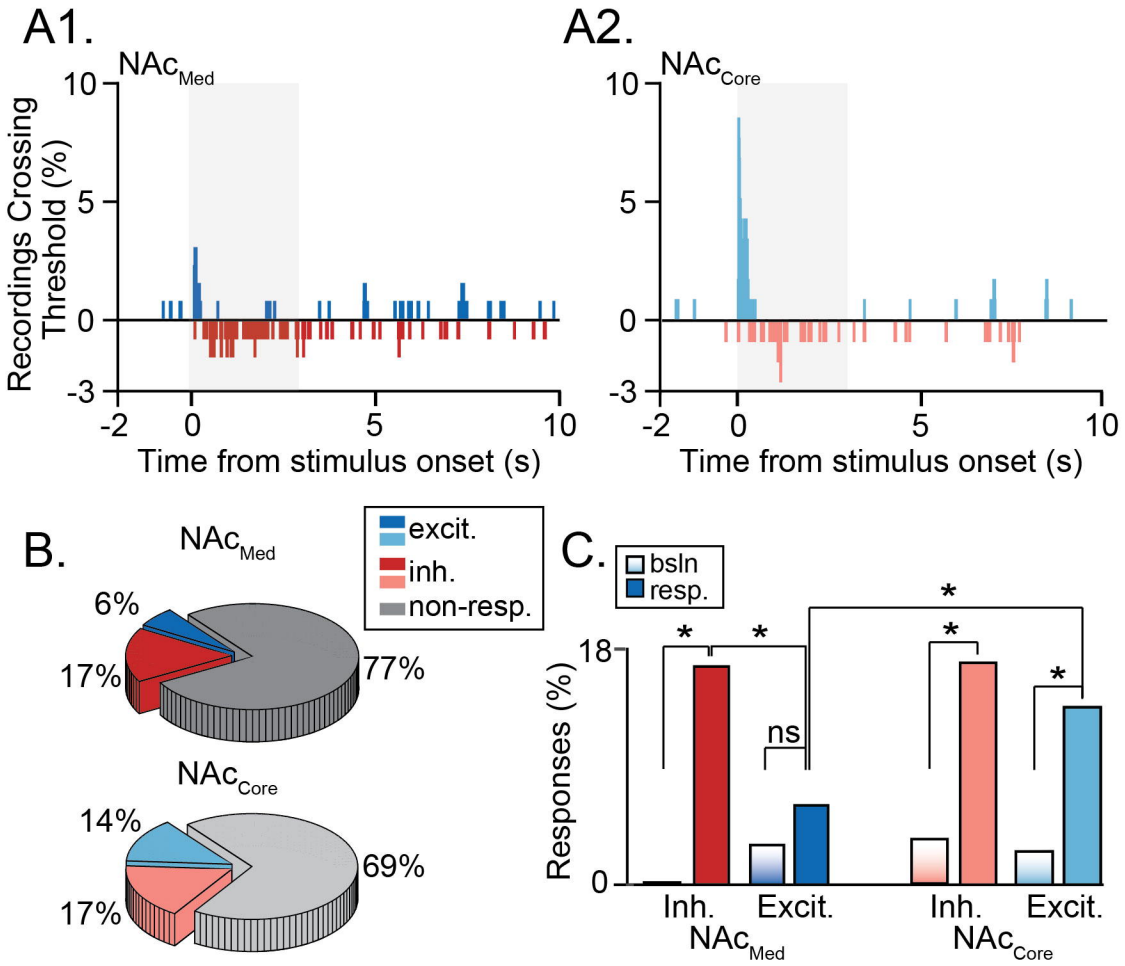

Figure 2

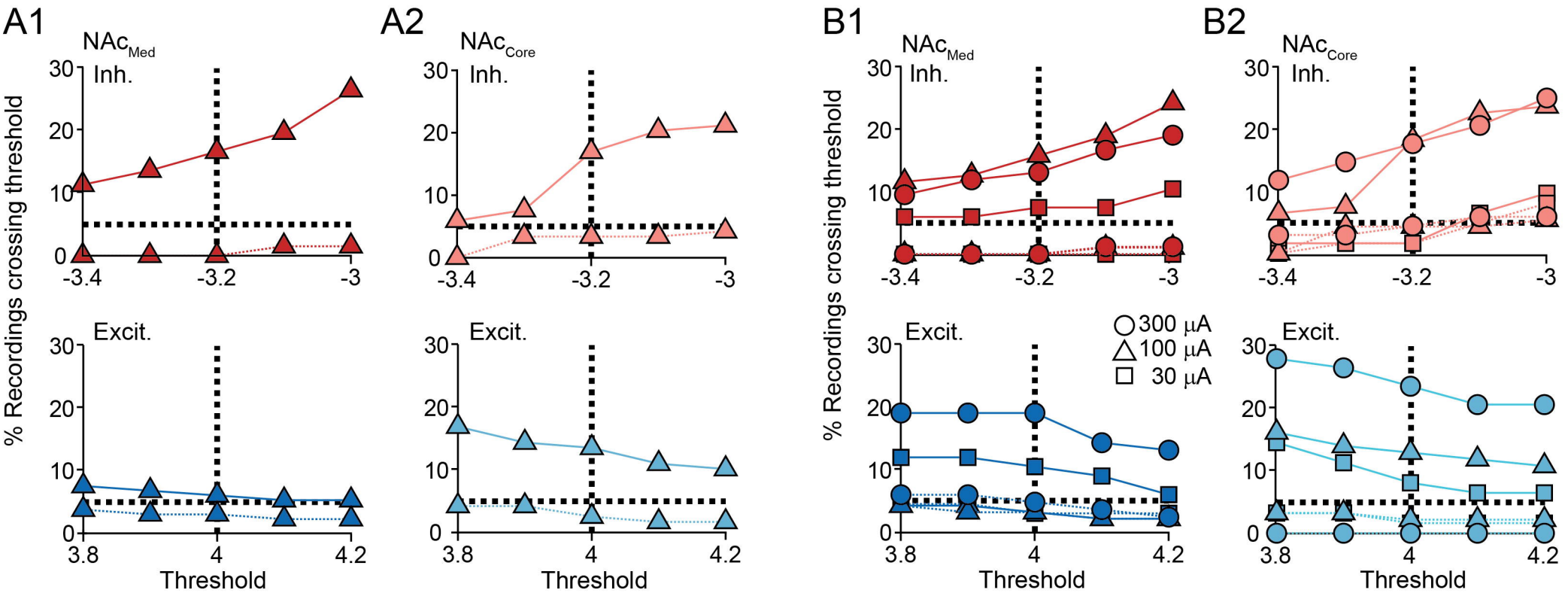
A1
A2
B1
B2
NAcMed
NAcCore
Inh.
Excit.
% Recordings crossing threshold
Threshold
300 μA
100 μA
30 μA

Figure 2S1

bioRxiv preprint doi: https://doi.org/10.1101/2020.09.28.283952; this version posted September 29, 2020. The copyright holder for this preprint (which was not certified by peer review) is the author/funder. All rights reserved. No reuse allowed without permission.

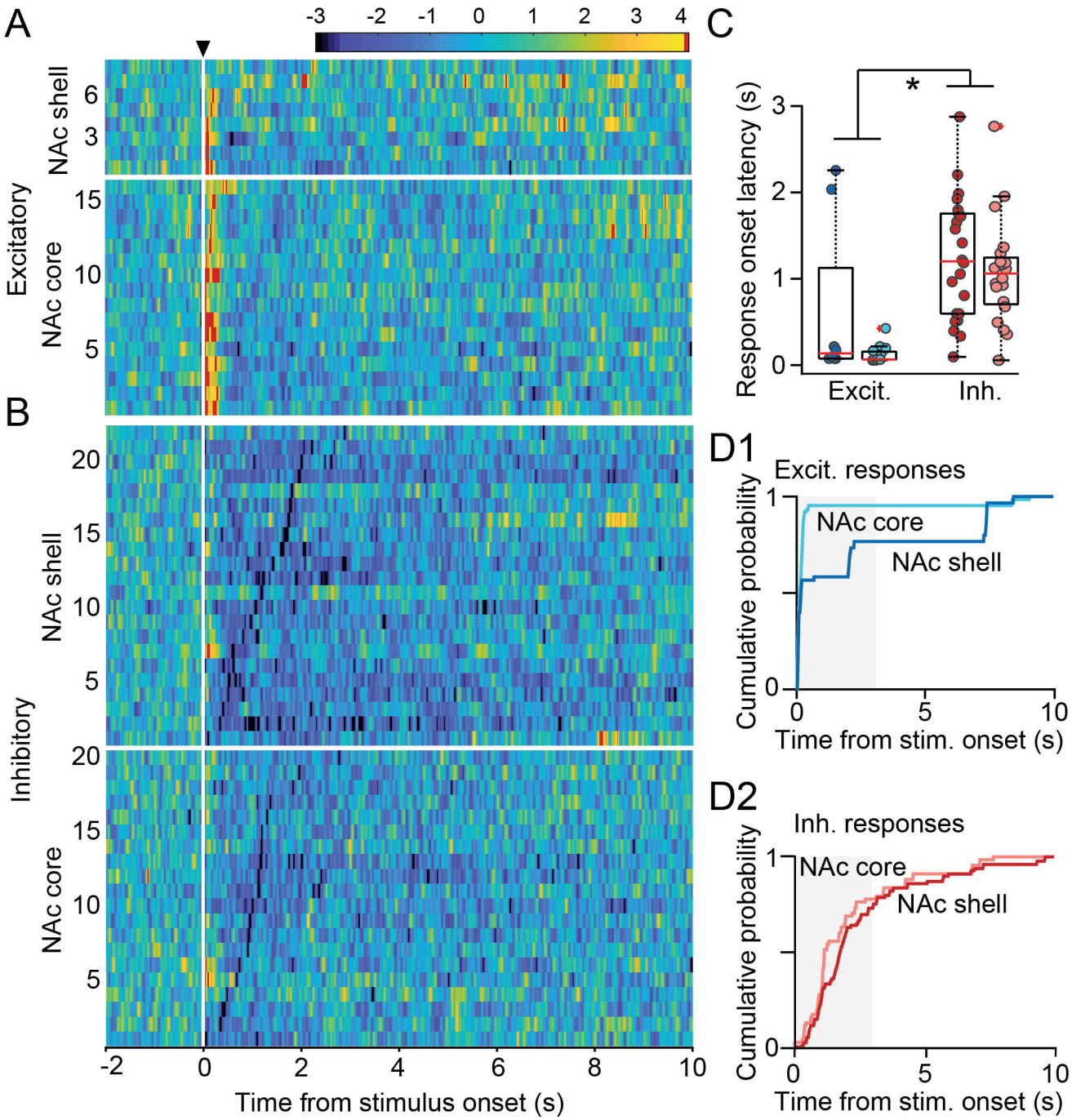

Figure 3

bioRxiv preprint doi: https://doi.org/10.1101/2020.09.28.283952; this version posted September 29, 2020. The copyright holder for this preprint (which was not certified by peer review) is the author/funder. All rights reserved. No reuse allowed without permission.

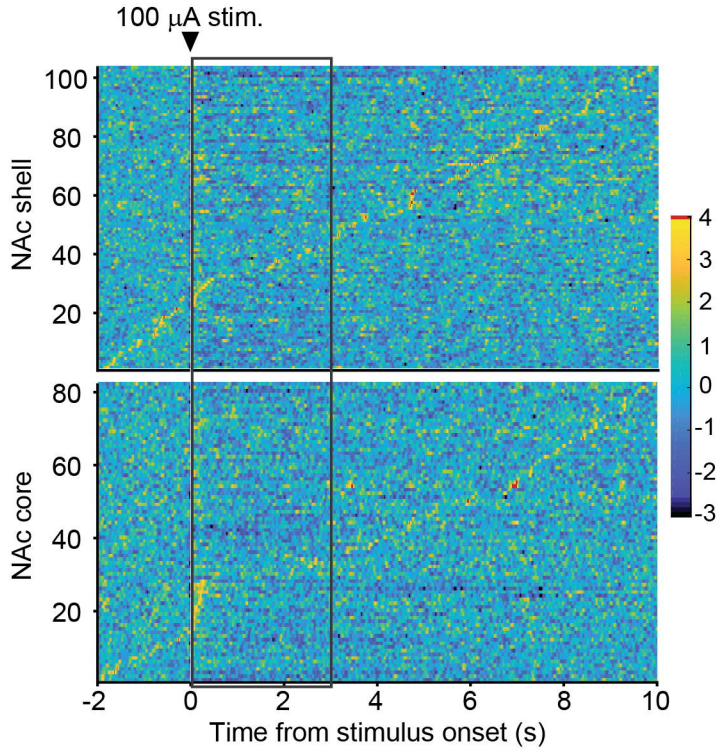

Figure 3S1

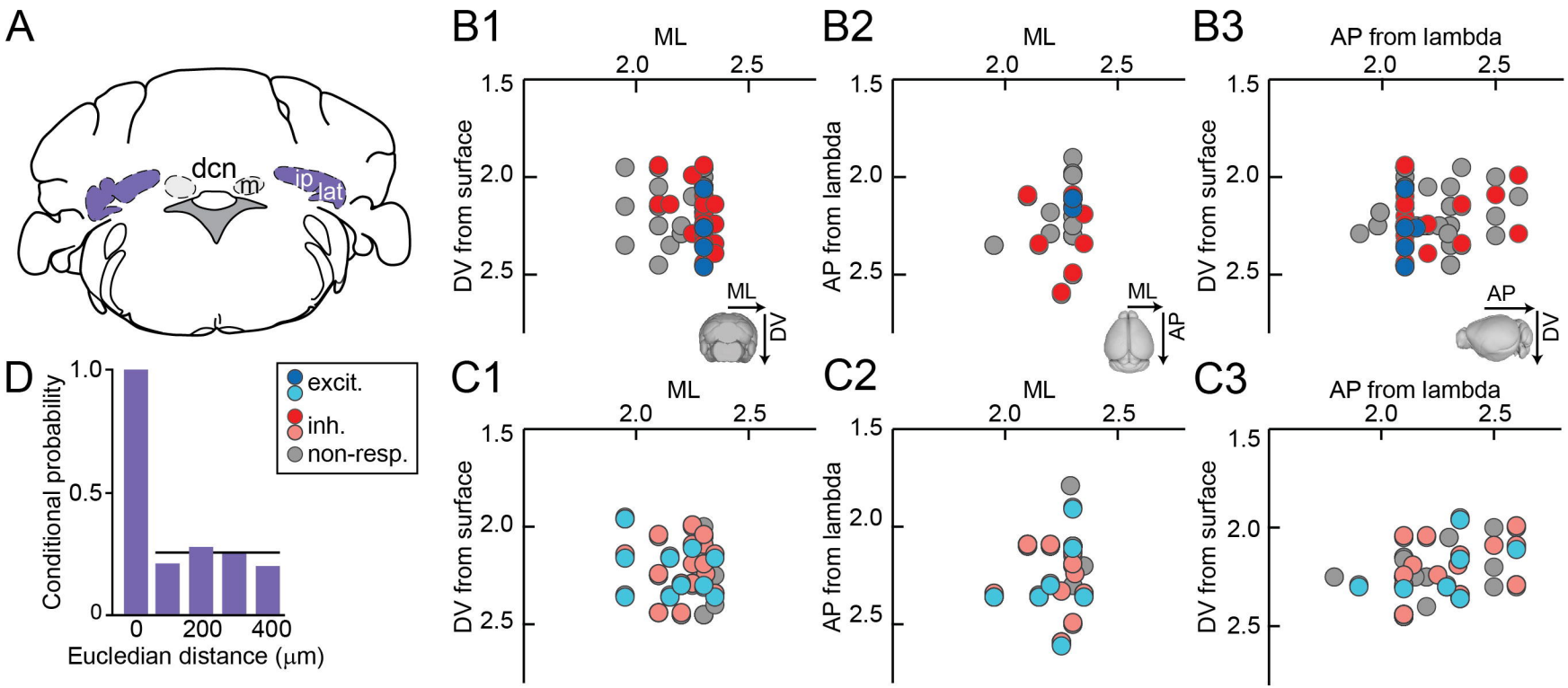
A
dcn
m
ip
lat
B1
ML
2.0
2.5
1.5
2.0
2.5
DV from surface
ML
DV
B2
ML
2.0
2.5
1.5
2.0
2.5
AP from lambda
ML
AP
B3
AP from lambda
2.0
2.5
1.5
2.0
2.5
DV from surface
AP
DV
D
1.0
0.5
0
Conditional probability
0
200
400
Eucledian distance (μm)
excit.
inh.
non-resp.
C1
ML
2.0
2.5
1.5
2.0
2.5
DV from surface
C2
ML
2.0
2.5
1.5
2.0
2.5
AP from lambda
C3
AP from lambda
2.0
2.5
1.5
2.0
2.5
DV from surface

Figure 4

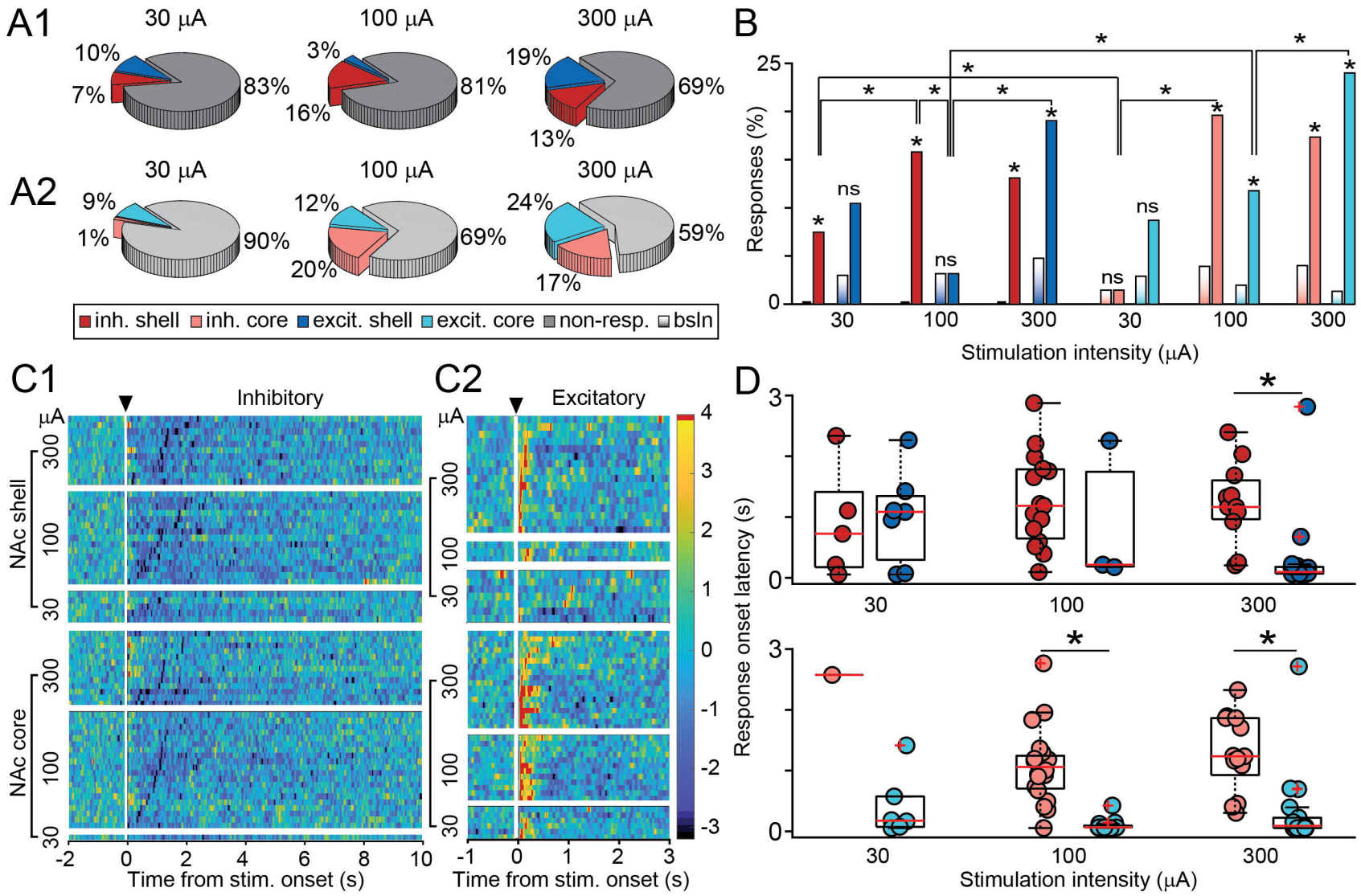
A1
30 μA
100 μA
300 μA
10%
7%
83%
3%
16%
81%
19%
13%
69%
A2
30 μA
100 μA
300 μA
9%
1%
90%
12%
20%
69%
24%
17%
59%
inh. shell
inh. core
excit. shell
excit. core
non-resp.
bsln
B
Responses (%)
25
0
ns
30
100
300
Stimulation intensity (μA)
C1
Inhibitory
μA
NAc shell
NAc core
Time from stim. onset (s)
C2
Excitatory
D
Response onset latency (s)
Stimulation intensity (μA)

Figure 5

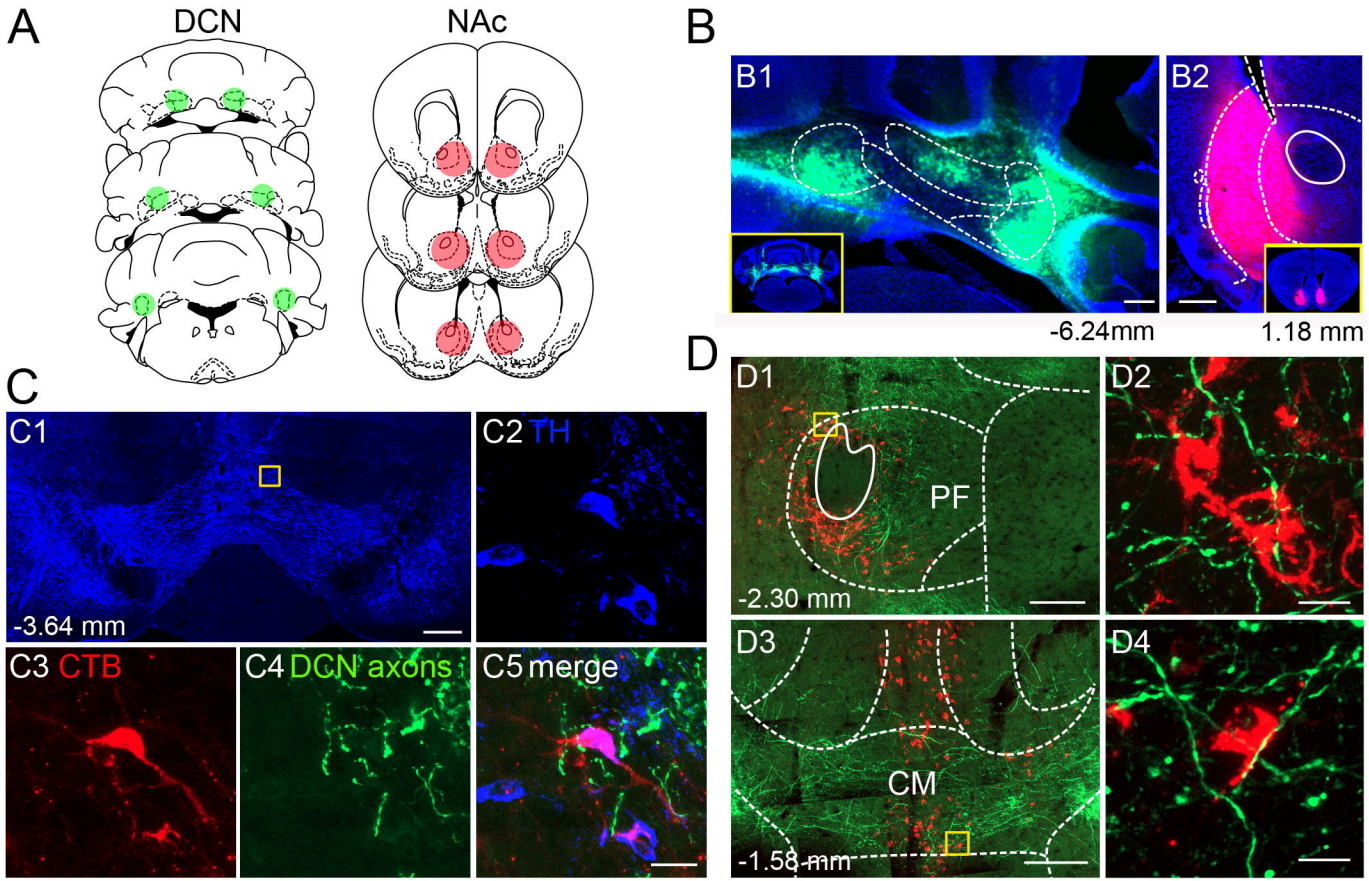
A
DCN
NAc
B
B1
B2
-6.24mm
1.18 mm
C
C1
-3.64 mm
C2 TH
C3 CTB
C4 DCN axons
C5 merge
D
D1
PF
-2.30 mm
D2
D3
CM
-1.58 mm
D4

Figure 6

bioRxiv preprint doi: https://doi.org/10.1101/2020.09.28.283952; this version posted September 29, 2020. The copyright holder for this preprint (which was not certified by peer review) is the author/funder. All rights reserved. No reuse allowed without permission.

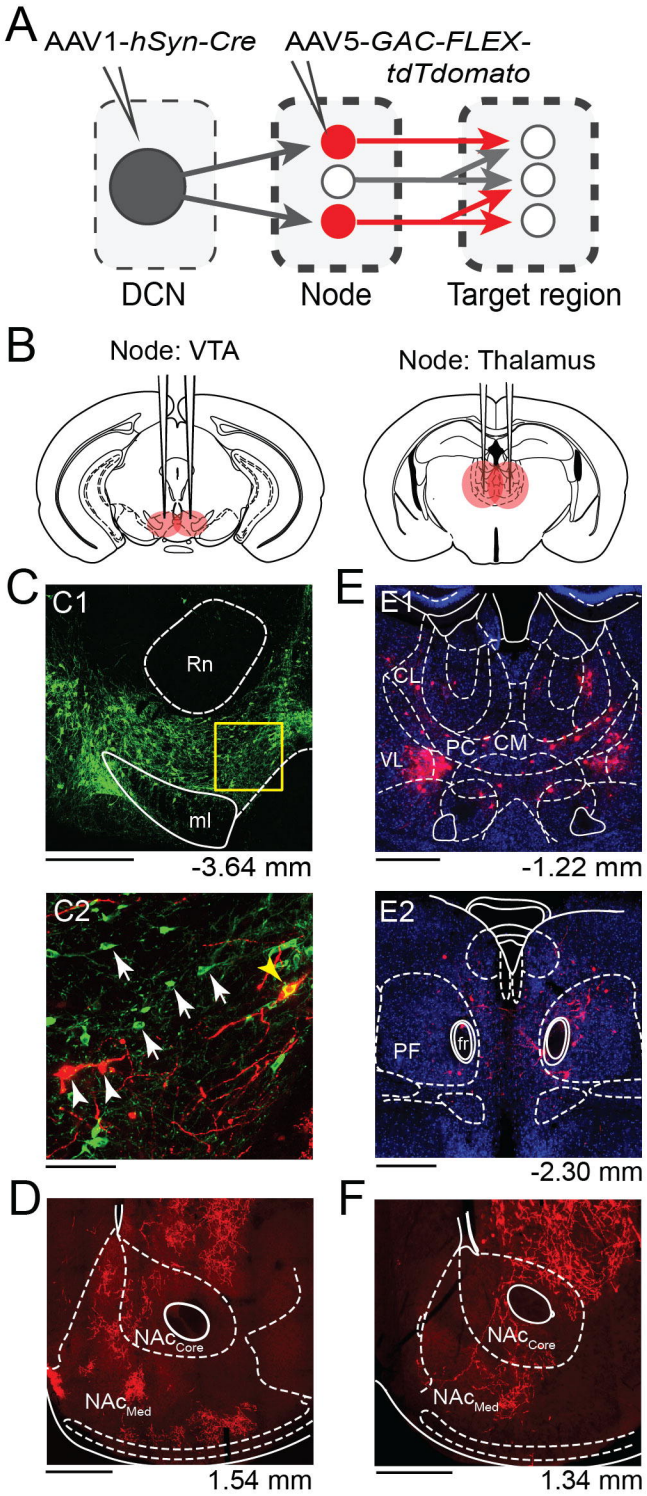

Figure 7